Upscaling of non-isothermal reactive porous media flow under dominant Péclet number : the effect of changing porosity

EINDHOVEN UNIVERSITY OF TECHNOLOGY
Department of Mathematics and Computer Science

CASA-Report 15-32
October 2015

Upscaling of non-isothermal reactive porous media flow under dominant Péclet number: the effect of changing porosity

by

C. Bringedal, I. Berre, I.S. Pop, F.A. Radu

Centre for Analysis, Scientific computing and Applications
Department of Mathematics and Computer Science
Eindhoven University of Technology
P.O. Box 513
5600 MB Eindhoven, The Netherlands
ISSN: 0926-4507

Upscaling of non-isothermal reactive porous media flow under dominant Péclet number: the effect of changing porosity

Carina Bringedal[1], Inga Berre[1,2], Iuliu Sorin Pop[1,3], and Florin Adrian Radu[1]

[1]Department of Mathematics, University of Bergen, PO Box 7800, 5020 Bergen, Norway
[2]Christian Michelsen Research AS, PO Box 6031, 5892 Bergen, Norway
[3]Centre for Analysis, Scientific Computing, and Applications, Eindhoven University of Technology, PO Box 513, 5600 MB Eindhoven, Netherlands
Carina.Bringedal@math.uib.no, Inga.Berre@math.uib.no, Florin.Radu@math.uib.no, i.pop@TUE.nl

Abstract

Motivated by rock-fluid interactions occurring in a geothermal reservoir, we present a two-dimensional pore scale model of a thin strip consisting of void space and grains, with fluid flow through the void space. Ions in the fluid are allowed to precipitate onto the grains, while minerals in the grains are allowed to dissolve into the fluid, taking into account the possible change in the aperture of the strip that these two processes cause. Temperature variations and possible effects of the temperature in both fluid density and viscosity and in the mineral precipitation and dissolution reactions are included. For the pore scale model equations, we investigate the limit as the width of the strip approaches zero, deriving one-dimensional effective equations. We assume that the convection is dominating over diffusion in the system, resulting in Taylor dispersion in the upscaled equations and a Forchheimer-type term in Darcy's law. Some numerical results where we compare the upscaled model with three simpler versions are presented; two still honoring the changing aperture of the strip but not including Taylor dispersion, and one where the aperture of the strip is fixed but contains dispersive terms.

1 Introduction

In a geothermal reservoir, cold water is injected and the warmer in-situ brine is produced. As the injected water and the in-situ brine have different temperatures and chemical composition, reservoir rock properties can develop dynamically with time as the fluids flow through the reservoir. Minerals dissolving and precipitating onto the reservoir matrix can change the porosity and hence the permeability of the system. Mineral solubility is affected by the cooling of the rock and by the different ion content in the saturating fluids, hence large changes in permeability can occur. This interaction among altering temperature, solute transport with mineral dissolution and precipitation and fluid flow is highly coupled and challenging to model appropriately as the relevant physical processes jointly affect each other [9]. As parameters affecting fluid flow can change through the production period, operating conditions for the geothermal plant are altered.

The ion content of the injected cold water is normally different than the original groundwater, affecting the equilibrium state of the chemical system. Field studies and simulations report porosity and permeability changes due to precipitation and dissolution of minerals as silica, quartz,

anhydrite, gypsum and calcite [16, 22, 23, 28, 37, 38]. Through modeling of the mineral precipitation and dissolution, we can better understand the processes and try to estimate to which extent the chemical reactions can affect the permeability in the porous medium.

The pore scale is highly relevant when modeling porosity changes as the reactions depend on the reactive surface area and the permeability depends on pore geometry. To invoke the pore scale effects, we start with a model on the pore scale and derive equations valid on Darcy scale by homogenization. Pore scale models incorporating mineral precipitation and dissolution have been studied earlier; e.g. in [32, 36] and the corresponding Darcy scale models have been investigated further in [14, 31]. These papers assume that the pore geometry is not changed by the chemical reactions, which is a valid assumption when the deposited or dissolved mineral layer is thin. Investigations honoring the porosity changes may be found in [7, 8, 15, 33, 34], where mineral precipitation and dissolution have been considered in a periodic porous medium or in a thin strip. In these papers, the position of the interface between grain and void space is tracked, giving a problem with a free boundary. Similar models can also be obtained for biofilm growth [35], for drug release from collagen matrices [27], and on an evolving microstructure [25].

In the present work we consider mineral precipitation and dissolution in a thin strip, which can represent a single pore channel in a geothermal reservoir. The strip can also be interpreted as a thin fracture surrounded by an impermeable medium. In the model, the effect of temperature on the chemical reactions and on the fluid flow is taken into account, giving a more coupled system of equations compared to previous works by van Noorden [34] and Kumar et al [15]. Temperature changes can initiate or accelerate the rate of chemical reactions due to changes in solubility of the minerals. Also, the fluid flow is affected by the temperature changes due to changes in the fluid density and viscosity. The model presented here builds on [7], but is extended to include a dominating convection, meaning that transport through fluid flow is happening at a shorter time scale than diffusive transport. This situation corresponds to the typical case for geothermal systems with water injection where water is injected at a high rate. The dominating convection is due to the large Péclet number appearing in the non-dimensional model. Such problems are considered in [3, 4, 5, 6, 10, 21, 19, 20], but in the case of fixed geometries, and in [15] in the variable geometry/free boundary context, but at isothermal conditions and hence for simpler flow models.

Using the pore scale model we can give an accurate description of the relevant processes, while upscaling the model to Darcy scale shows which pore scale effects are important at a larger scale, and how these processes are coupled. Extending the previously considered pore scale model in [7] to include a large Péclet number means that other pore scale processes gain importance at the Darcy scale. Kumar et al [15] did a similar extension of the thin strip in [34] and could therefore observe Taylor dispersion [30]. Compared to fixed geometry models including Taylor dispersion; such as [20], Kumar et al [15] also found how the transport was affected by the reactions. Taylor dispersion and coupling between transport and reactions at the Darcy scale are also important processes in the present work, but further effects will appear due to the couplings with temperature dependence.

The structure of this paper is as follows: In Section 2 we present the pore scale model, while in Section 3 we perform formal homogenization on the model equations, obtaining one-dimensional upscaled equations. Some numerical examples are shown in Section 4. The paper ends with some concluding remarks on the resulting upscaled equations in Section 5.

2 Pore scale model

The thin strip is shown in Figure 1. The length of the strip is L while the width is l, where l is much smaller than L. Symmetry around the horizontal axis is assumed. The width of the mineral part is $d(x,t)$, where $0 \leq d(x,t) < l/2$, hence clogging is not allowed.

The total domain Υ is the rectangle seen in the figure given by

$$\Upsilon = \{(x,y) \in R^2 |\ 0 \leq x \leq L, -l/2 \leq y \leq l/2\}.$$

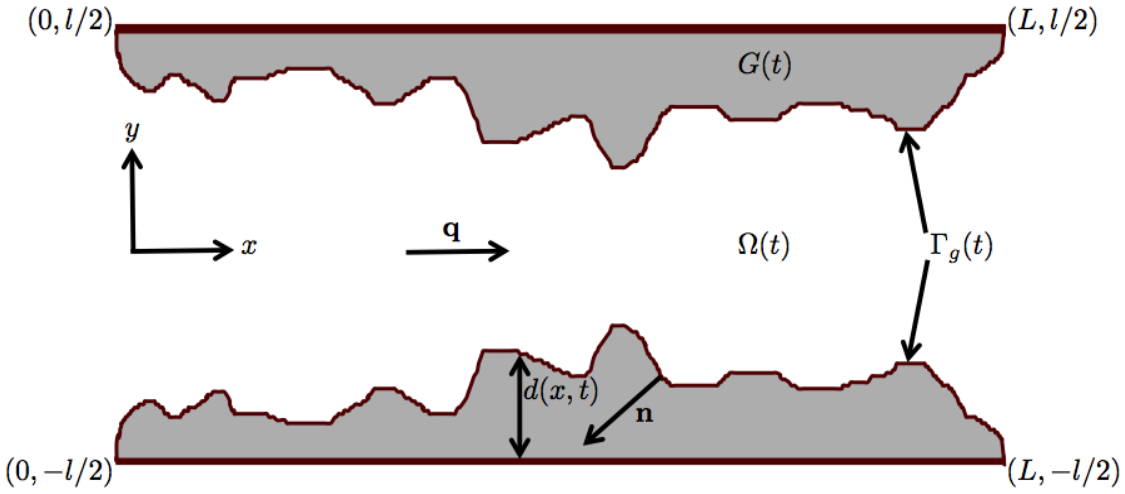

Figure 1: Model of thin strip.

The void space $\Omega(t)$ where fluid can flow is defined by

$$\Omega(t) = \{(x, y) \in R^2 |\ 0 \leq x \leq L, -(l/2 - d(x,t)) \leq y \leq (l/2 - d(x,t))\},$$

while the grain space $G(t)$ consisting of minerals is

$$G(t) = \{(x, y) \in R^2 |\ 0 \leq x \leq L, -l/2 \leq y \leq -(l/2 - d(x,t)) \vee (l/2 - d(x,t)) \leq y \leq l/2\}.$$

The interface $\Gamma_g(t)$ where mineral precipitation and dissolution can occur, is given by

$$\Gamma_g(t) = \{(x, y) \in R^2 |\ 0 < x < L, y = \pm(l/2 - d(x,t))\}.$$

The outward unit normal $\mathbf{n}$ of the interface is (for the lower part) given by

$$\mathbf{n} = (\partial_x d, -1)^T / \sqrt{1 + (\partial_x d)^2}.$$

As the mineral width $d(x,t)$ changes with time, a point located at the interface $\Gamma_g(t)$ has a certain velocity. A point at the interface has coordinates $\mathbf{s}(t) = (x(t), -(l/2 - d(x,t)))$ and velocity $\mathbf{s}'(t) = (x'(t), \partial_x d x'(t) + \partial_t d)$ by the chain rule. Hence, the normal velocity of the lower boundary is

$$v_n = \mathbf{n} \cdot \mathbf{s}'(t) = -\partial_t d / \sqrt{1 + (\partial_x d)^2}. \tag{1}$$

The Rankine-Hugoniot condition guarantees conservation of quantities across a moving boundary [13]:

$$\mathbf{n} \cdot [\mathbf{j}] = v_n [u] \tag{2}$$

where u is the preserved quantity (e.g. mass or energy) and $\mathbf{j}$ is the flux of this quantity. The use of square brackets means the *jump* of the quantities, and is the difference between the quantities at each side of the interface; $[u] = u^+ - u^-$, where the positive and negative side are chosen according to the orientation of the normal vector $\mathbf{n}$ [13].

We assume conservation of ions, mass, momentum and energy to form a complete set of equations and refer readers to e.g. [24] for justification of the conservation equations. Boundary conditions at the internal boundary and otherwise at the external boundaries are prescribed when necessary for the upscaling process. For computer simulations, more external boundary conditions and initial conditions are required. As these are not necessary for the upscaling process, they will not be specified in this section.

2.1 Conservation of ions

There are two active ions in the fluid, with molar concentrations u^1 and u^2. They satisfy the convection-diffusion equation in the void space:

$$\partial_t u^i = \nabla \cdot (D\nabla u^i - \mathbf{q}u^i) \text{ for } (x, y) \in \Omega(t). \tag{3}$$

In the above equation, D is the diffusion coefficient, which we assume to be constant, and $\mathbf{q}$ is the fluid velocity. The Rankine-Hugoniot condition (2) for conserving ions across the moving interface is

$$\mathbf{n} \cdot (D\nabla u^i - \mathbf{q}u^i) = v_n(\rho_C - u^i) \text{ on } \Gamma_g(t), \tag{4}$$

where ρ_C is the molar density of the formed solid. The difference on the right-hand is the jump of ion concentration: the ions are either dissolved in the fluid space with molar concentration u^i or as part of the mineral molecules with molar density ρ_C. The two ions are assumed to have initially the same concentration. As the same number of ions disappear or are produced through the reaction, the two ions will always have the same concentration. Hence, $u^1 = u^2 = u$.

2.2 Conservation of mass

The fluid consists of water and the two dissolved components. As the fluid consists mainly of water, the fluid molar density ρ_f is assumed to not be affected by the chemical reactions, but depends on temperature. The same holds also for the fluid viscosity, μ. These dependencies are made specific in (32) below. Hence, the mass conservation equation of the fluid is

$$\partial_t \rho_f + \nabla \cdot (\rho_f \mathbf{q}) = 0 \text{ for } (x, y) \in \Omega(t). \tag{5}$$

At the boundary, ions can leave the fluid and become part of the grain space instead. The Rankine-Hugoniot boundary condition applied to mass is

$$\mathbf{n} \cdot (-\rho_f \mathbf{q}) = v_n(2\rho_C - \rho_f) \text{ on } \Gamma_g(t). \tag{6}$$

The factor $(2\rho_C - \rho_f)$ describes the jump of the mass. As a mineral molecule consists of two ions that can be released into or retrieved from the fluid, the factor 2 appears in front of ρ_C. Note that if $\rho_f \equiv 2\rho_C$, the normal component of the velocity is zero at the interface, meaning that the chemical reactions do not cause volume change. This simplifying assumption is made in, e.g., [15], but would be inconsistent with our assumptions of varying fluid density and constant grain density.

2.3 Conservation of momentum

Conservation of momentum can be expressed as

$$\begin{aligned} \partial_t(\rho_f \mathbf{q}) + \nabla \cdot (\rho_f \mathbf{q}\mathbf{q}) = &- \nabla p + \nabla \cdot \Big(\mu(\nabla \mathbf{q} + (\nabla \mathbf{q})^T)\Big) \\ &- \frac{2}{3}\nabla(\mu \nabla \cdot \mathbf{q}) \text{ for } (x, y) \in \Omega(t), \end{aligned} \tag{7}$$

where we have assumed that the fluid is Newtonian and isotropic and that the stress tensor is a linear function of the strain rates. We apply no-slip conditions at the interface in the sense that the velocity $\mathbf{q}$ is assumed to have zero tangential component at the interface. As the interface can move in the normal direction, we allow the fluid to have a normal component. Combining with equation (6), the new boundary condition becomes

$$\mathbf{q} = \frac{\rho_f - 2\rho_C}{\rho_f} v_n \mathbf{n} \text{ on } \Gamma_g(t). \tag{8}$$

2.4 Conservation of energy

We separate between two temperatures; the temperature in the fluid T_f and temperature in the grain T_g. The separation is made to emphasize the different heat transfer processes occurring in the two domains. Fluid temperature is only defined in the void space $\Omega(t)$ and grain temperature is defined in the grain space $G(t)$. We assume no viscous dissipation, hence energy transfer in the fluid can happen through diffusion and convection, which gives the temperature equation

$$\partial_t(\rho_f c_f T_f) = \nabla \cdot (k_f \nabla T_f - \rho_f c_f \mathbf{q} T_f) \text{ in } \Omega(t). \tag{9}$$

In the grain space flow is not possible, hence

$$\partial_t(\rho_C c_g T_g) = \nabla \cdot (k_g \nabla T_g) \text{ in } G(t). \tag{10}$$

In the above equations, c_f and c_g are specific heats, and k_f and k_g are heat conductivities, of fluid and mineral respectively, and are all assumed constant. The Rankine-Hugoniot condition for conservation of energy across the moving interface is

$$\mathbf{n} \cdot (k_f \nabla T_f - \rho_f c_f \mathbf{q} T_f - k_g \nabla T_g) = v_n(\rho_C c_g T_g - \rho_f c_f T_f) \text{ on } \Gamma_g(t), \tag{11}$$

and we also assume temperature continuity at the interface; that is,

$$T_g = T_f \text{ on } \Gamma_g(t). \tag{12}$$

For the lower and upper part of $G(t)$, homogeneous Neumann boundary conditions is assumed; hence,

$$\partial_y T_g = 0 \text{ for } 0 \le x \le L, y = \pm l/2. \tag{13}$$

2.5 How reactions affect the grain width

At the interface $\Gamma_g(t)$, minerals can precipitate and dissolve. The position of the boundary changes continuously throughout this process. This change is quantified through changes in the grain width $d(x,t)$ and the normal velocity v_n. The normal velocity is proportional to the local difference between dissolution and precipitation rates,

$$\rho_C v_n = -(f_p - f_d) \text{ on } \Gamma_g(t), \tag{14}$$

where f_p and f_d are the precipitation and dissolution rates for the reaction. The precipitation rate is assumed to increase with ion concentration and with temperature. This is described through a kinetic rate depending on ion concentration with an Arrhenius factor [11, 34],

$$f_p(T_f, u) = k_0 e^{-E/RT_f} \frac{u^2}{K_m(T_f)}, \tag{15}$$

where k_0 is a positive rate constant, E is the activation energy, R is the gas constant, T_f is fluid temperature and $K_m(T_f)$ is the equilibrium constant for the mineral. The equilibrium constant is allowed to vary with fluid temperature, but is constant in the sense that it is independent of ion and mineral concentration. Dissolution can take place as long as there are precipitated minerals present; that is, as long as $d(x,t) > 0$. We assume that the dissolution happens faster at higher temperatures, hence

$$f_d(T_f, u, d) = k_0 e^{-E/RT_f} w(d(x,t), T_f, u), \tag{16}$$

where $w(d, T_f, u)$ is given by

$$w(d, T_f, u) = \begin{cases} 0 & \text{if } d < 0 \\ \min(\frac{u^2}{K_m(T_f)}, 1) & \text{if } d = 0 \\ 1 & \text{if } d > 0. \end{cases}$$

Collecting the equations (14), (15) and (16) and combining with (1), yields

$$\rho_C \partial_t d(x,t) = k_0 e^{-E/RT_f} \Big(\frac{u^2}{K_m(T_f)} - w(d(x,t), T_f, u) \Big) \sqrt{1 + (\partial_x d(x,t))^2} \text{ on } \Gamma_g(t). \tag{17}$$

This equation describes how the reaction rates affect the aperture through the derivatives of the mineral width $d(x,t)$.

2.6 Non-dimensional equations

To achieve non-dimensional quantities, we introduce t_{ref}, $x_{ref} = L$, $y_{ref} = l$, u_{ref}, q_{ref}, $p_{ref} = L^4 u_{ref}/t_{ref}^2 l^2$, T_{ref}, $\mu_{ref} = l^2 p_{ref}/L q_{ref}$ and let $\epsilon = l/L$. Non-dimensional quantities are denoted with a hat and are defined as

$$\begin{aligned}
\hat{t} &= t/t_{ref}, & \hat{x} &= x/x_{ref}, & \hat{y} &= y/y_{ref}, & \hat{u}^\epsilon &= u/u_{ref}, \\
\hat{\mathbf{q}}^\epsilon &= \mathbf{q}/q_{ref}, & \hat{p}^\epsilon &= p/p_{ref}, & \hat{\rho}_f &= \rho_f/u_{ref}, & \hat{\rho} &= \rho_C/u_{ref}, \\
\hat{d}^\epsilon &= d/y_{ref}, & \hat{\mu} &= \mu/\mu_{ref}, & \hat{T_f}^\epsilon &= T_f/T_{ref}. & \hat{T_g}^\epsilon &= T_g/T_{ref}
\end{aligned}$$

Dependence on the small variable ϵ is emphasized by denoting our main variables with ϵ as a superscript. Observe that the dimensionless viscosity scales with ϵ^2, which is a natural assumption when upscaling of porous media flows (see e.g. [2] or [17]) and is also the context used in [29] for proving rigorously the convergence of the homogenization process. This assumption leads to non-trivial upscaled flows when ϵ approaches zero. In this case, the friction of the fluid at the pore walls, where no-slip conditions are assumed, is balanced by either a lower viscosity, or a high pressure exerted to set the fluid in motion, or a low fluid velocity.

The reference time for fluid flow is $t_F = L/q_{ref}$ and will also act as reference time for observations; t_{ref}. Further, the reference time for solute diffusion is $t_D = L^2/D$, heat conduction (for the fluid phase) is $t_C = L^2 u_{ref} c_f/k_f$ and the reference time for chemical reactions is $t_R = u_{ref} l/k_0$. Using these reference times we define two Péclet numbers and the Damköhler number:

$$Pe_D = \frac{t_D}{t_F} = O(\epsilon^{-\beta_1}) \quad Pe_C = \frac{t_C}{t_F} = O(\epsilon^{-\beta_2}) \quad Da = \frac{t_F}{t_R} = O(\epsilon^{\beta_3}).$$

As the model is convection dominated, β_1 and β_2 will be positive, giving large Péclet numbers. Using values representative for a geothermal system, it is reasonable to assume $\beta_1 = \beta_2 = 1$ and $\beta_3 = 0$. This way the non-dimensional solute diffusion parameter, heat conduction parameters and reactive parameter are

$$\hat{D} = \epsilon^{-1} \frac{D}{L q_{ref}}, \quad \hat{\kappa}_f = \epsilon^{-1} \frac{k_f}{L u_{ref} q_{ref} c_f}, \quad \hat{\kappa}_g = \epsilon^{-1} \frac{k_g}{L u_{ref} q_{ref} c_f} \quad \hat{k} = \epsilon^0 \frac{k_0 L}{q_{ref} u_{ref} l}.$$

Observe that choosing the dimensionless fluid density $\hat{\rho}_f$ as the ratio of the fluid molar density ρ_f and the reference species molar density u_{ref} implicitly means that u_{ref} is the reference value for the fluid molar density. Together with the chosen reference time t_{ref} and pressure p_{ref}, one immediately obtains $\mu_{ref} = L u_{ref} q_{ref}$.

Since from now on we will only use non-dimensional variables, we skip the hat in the notations and all quantities and variables below should be understood as non-dimensional.

Using non-dimensional variables, the total domain is defined by

$$\Upsilon^\epsilon = \{(x,y) \in R^2 \mid 0 \le x \le 1, -1/2 \le y \le 1/2\}.$$

The void space is now given by

$$\Omega^\epsilon(t) = \{(x,y) \in R^2 \mid 0 \le x \le 1, -(1/2 - d^\epsilon(x,t)) \le y \le (1/2 - d^\epsilon(x,t))\},$$

while the grain space is defined as

$$G^\epsilon(t) = \{(x,y) \in R^2 \mid 0 \le x \le 1, -1/2 \le y \le -(1/2 - d^\epsilon) \vee (1/2 - d^\epsilon) \le y \le 1/2\}.$$

The interface between the void and grain space is now

$$\Gamma^\epsilon(t) = \{(x,y) \in R^2 \mid 0 \le x \le 1, y = \pm(1/2 - d^\epsilon(x,t))\},$$

while the outward unit normal for the lower part of the interface is given by

$$\mathbf{n}^\epsilon = (\epsilon\partial_x d^\epsilon, -1)^T / \sqrt{1 + (\epsilon\partial_x d^\epsilon)^2}. \tag{18}$$

Inserting the dimensionless variables into the model equations gives the following set of equations and boundary conditions. The normal velocity v_n is inserted from equation (1) when necessary. Note that due to different scaling in the two spatial directions, the ∇-operator is defined as $\nabla = \frac{\partial}{\partial x}\mathbf{i} + \frac{1}{\epsilon}\frac{\partial}{\partial y}\mathbf{j}$.

The convection-diffusion equation (3) describing the ion concentration becomes

$$\partial_t u^\epsilon + \nabla \cdot (\mathbf{q}^\epsilon u^\epsilon) = \epsilon D \nabla^2 u^\epsilon \text{ in } \Omega^\epsilon(t), \tag{19}$$

with the boundary condition (4) now written as

$$\mathbf{n}^\epsilon \cdot (\epsilon D \nabla u^\epsilon - \mathbf{q}^\epsilon u^\epsilon) = -\epsilon \partial_t d^\epsilon (\rho - u^\epsilon)/\sqrt{1 + (\epsilon\partial_x d^\epsilon)^2} \text{ on } \Gamma^\epsilon(t). \tag{20}$$

Note that an underlying assumption is that the non-dimensional diffusion coefficient D is of order 1, and the difference in representative time scales appears as the factor ϵ in front of D. This assumption on D is to ensure we are still in the regime of the Péclet number being $O(\epsilon^{-1})$.

The mass conservation equation (5) transforms into

$$\partial_t \rho_f + \nabla \cdot (\rho_f \mathbf{q}^\epsilon) = 0 \text{ in } \Omega^\epsilon(t). \tag{21}$$

The non-dimensional Rankine-Hugoniot boundary equation (6) is

$$\mathbf{q}^\epsilon \cdot \mathbf{n}^\epsilon = -\epsilon \frac{\rho_f - 2\rho}{\rho_f} \partial_t d^\epsilon / \sqrt{1 + (\epsilon\partial_x d^\epsilon)^2} \text{ on } \Gamma^\epsilon(t). \tag{22}$$

The momentum balance equation (7) becomes

$$\begin{aligned} \epsilon^2 \Big(\partial_t(\rho_f \mathbf{q}^\epsilon) + \nabla \cdot (\rho_f \mathbf{q}^\epsilon \mathbf{q}^\epsilon) \Big) &= -\nabla p^\epsilon \\ &+ \epsilon^2 \Big(\nabla \cdot \Big(\mu(\nabla \mathbf{q}^\epsilon + (\nabla \mathbf{q}^\epsilon)^T) \Big) - \frac{2}{3} \nabla(\mu \nabla \cdot \mathbf{q}^\epsilon) \Big) \text{ in } \Omega^\epsilon(t). \end{aligned} \tag{23}$$

The factor ϵ^2 in the above appears due to the chosen scaling of the (reference) viscosity, pressure and time. While having a viscosity of order ϵ^2 leads to non-trivial upscaled models, the scaling of the time derivative and inertia terms is important as well and can lead to different variants of the (Darcy like) models. Such aspects are discussed in [1, 2, 18]. The boundary condition (8) is

$$\mathbf{q}^\epsilon = -\epsilon \frac{\rho_f - 2\rho}{\rho_f} \partial_t d^\epsilon \mathbf{n}^\epsilon / \sqrt{1 + (\epsilon\partial_x d^\epsilon)^2} \text{ on } \Gamma^\epsilon(t). \tag{24}$$

The non-dimensional forms of the energy conservation equations (9) and (10) are

$$\partial_t(\rho_f T_f^\epsilon) + \nabla \cdot (\rho_f \mathbf{q}^\epsilon T_f^\epsilon) = \epsilon \kappa_f \nabla^2 T_f^\epsilon \text{ in } \Omega^\epsilon(t) \tag{25}$$

and

$$\partial_t(\varsigma \rho T_g^\epsilon) = \epsilon \kappa_g \nabla^2 T_g^\epsilon \text{ in } G^\epsilon(t), \tag{26}$$

where $\varsigma = c_g/c_f$, κ_f and κ_g are assumed to be of order 1. The assumption on ς is to ensure the heat exchange rate in fluid and solid to not deviate too much, and is a typical choice for most

relevant solids. Further, the assumptions on κ_f and κ_g follow from the assumption on the Péclet number being $O(\epsilon^{-1})$. The boundary condition (11) is written

$$\begin{aligned}\mathbf{n}^\epsilon \cdot (\epsilon\kappa_f \nabla T_f^\epsilon - \rho_f \mathbf{q}^\epsilon T_f^\epsilon - \epsilon\kappa_g \nabla T_g^\epsilon) \\ = -\epsilon(\varsigma\rho T_g^\epsilon - \rho_f T_f^\epsilon)\partial_t d^\epsilon / \sqrt{1 + (\epsilon\partial_x d^\epsilon)^2} \text{ on } \Gamma^\epsilon(t),\end{aligned} \tag{27}$$

and the continuity condition (12) is

$$T_g^\epsilon = T_f^\epsilon \text{ on } \Gamma^\epsilon(t). \tag{28}$$

The boundary condition (13) for T_g is now

$$\partial_y T_g^\epsilon = 0 \text{ for } 0 \leq x \leq 1, y = \pm 1/2. \tag{29}$$

The non-dimensional version of the equation (17) is

$$\rho\partial_t d^\epsilon = (f_p(T_f^\epsilon, u^\epsilon) - f_d(T_f^\epsilon, u^\epsilon, d^\epsilon))\sqrt{1 + (\epsilon\partial_x d^\epsilon)^2} \text{ on } \Gamma^\epsilon(t). \tag{30}$$

The reaction rates are non-dimensional and are given by

$$f_p(T_f^\epsilon, u^\epsilon) = k e^{-\alpha/T_f^\epsilon} \frac{(u^\epsilon)^2}{K_m(T_f^\epsilon)}$$

and

$$f_d(T_f^\epsilon, u^\epsilon, d^\epsilon) = k e^{-\alpha/T_f^\epsilon} w(d^\epsilon(x,t), T_f^\epsilon, u^\epsilon), \tag{31}$$

where $\alpha = E/RT_{ref}$ is non-dimensional. Also note that $K_m(T_f^\epsilon)$ is non-dimensionalized. The non-dimensional reactive constant k is of order 1 due to the previous assumption on the Damköhler number.

The fluid density and viscosity are assumed to depend linearly on the fluid temperature T_f^ϵ, hence

$$\rho_f(T_f^\epsilon) = \rho_0 - \beta_{\rho_f} T_f^\epsilon \text{ and } \mu(T_f^\epsilon) = \mu_0 - \beta_\mu T_f^\epsilon, \tag{32}$$

for some positive constants β_{ρ_f} and β_μ and reference density and viscosity ρ_0 and μ_0. The assumption of linear dependence is a common simplification, but using other differentiable dependencies between density/viscosity and temperature is straightforward through Taylor expanding the relationships. Using linear relationships simplifies the presentation of the upscaling steps, but the resulting model is not explicitly dependent on using these linear models for density and viscosity. The considered temperature range is such that the fluid density is decreasing with temperature; hence, the dimensional temperature should correspond to above $4°C$, and otherwise below temperatures that would result in boiling. Note that the two constants β_{ρ_f} and β_μ are relatively small, but are assumed to be independent of ϵ to avoid over-simplyfing the potential dependence.

3 Asymptotic expansion

We perform a formal asymptotic expansion for the variables depending on ϵ, namely u^ϵ, d^ϵ, $\mathbf{q}^\epsilon$, p^ϵ, T_f^ϵ and T_g^ϵ. For all expecting d^ϵ we assume

$$u^\epsilon(x,y,t) = u_0(x,y,t) + \epsilon u_1(x,y,t) + O(\epsilon^2),$$

where $u_0(x,y,t)$ is the function describing the first order behavior of the variable u^ϵ. The following term $\epsilon u_1(x,y,t)$ is less important as ϵ is small. Since the velocity $\mathbf{q}^\epsilon$ is a vector function, we apply the above expansion for both the horizontal component $q^{\epsilon(1)}$ and the vertical component $q^{\epsilon(2)}$. The width d^ϵ does not depend on y and has the expansion

$$d^\epsilon(x,t) = d_0(x,t) + \epsilon d_1(x,t) + O(\epsilon^2).$$

Below we follow the ideas in [7] and [15]. The goal is to derive an upscaled effective model describing the thin strip with vanishing width, obtaining a one-dimensional model still honoring the changes in aperture. Collecting the lowest order terms as in [7] would result in a hyperbolic model due to the dominating convection. The hyperbolic model could be a poor approximation to the original equations [15], hence we include the second lowest order variables u_1, d_1, etc, as well in the upscaling process.

3.1 Conservation of mass part I

The required asymptotic expansions are inserted into the mass conservation equation (21). Although we have not shown it yet, we will take advantage of T_{f0} being independent of y. We make use of the notation $\rho_{f0} = \rho_0 - \beta_{\rho_f} T_{f0}$. The lowest order term is

$$\partial_y(\rho_{f0} q_0^{(2)}) = 0,$$

and, since ρ_{f0} is independent of y, this means that $\partial_y q_0^{(2)} = 0$. The second lowest order terms are

$$\partial_t \rho_{f0} + \partial_x(\rho_{f0} q_0^{(1)}) + \partial_y(\rho_{f0} q_1^{(2)}) = 0. \tag{33}$$

Sorted into order and components, the boundary condition (24) arising from the momentum balance equation expresses that

$$q_0^{(1)} = 0, \quad q_0^{(2)} = 0, \quad q_1^{(1)} = 0, \quad q_1^{(2)} = -\frac{2\rho - \rho_{f0}}{\rho_{f0}} \partial_t d_0 \quad \text{for } y = \pm(\frac{1}{2} - d_0). \tag{34}$$

As $\partial_y q_0^{(2)} = 0$ in the void space, we conclude that

$$q_0^{(2)} \equiv 0.$$

To proceed, the mass conservation equation (21) is integrated across a thin section in the void space with width δx; the integration area is given by $Y = \{(x, y) \in R^2 \mid x_1 \le x \le x_1 + \delta x, -(1/2 - d^\epsilon) \le y \le 1/2 - d^\epsilon\}$. Hence, we obtain

$$0 = \int_Y \partial_t \rho_f dV + \int_Y \nabla \cdot (\rho_f \mathbf{q}^\epsilon) dV.$$

Gauss' theorem is applied to the second integral and the whole equation is divided by δx at the same time. We insert the limits in our two integrals accordingly, apply the asymptotic expansions and keep terms up to $O(\epsilon^2)$, hence obtaining

$$\begin{aligned} O(\epsilon^2) = \frac{1}{\delta x} \int_{x_1}^{x_1+\delta x} \int_{-(1/2-d_e)}^{1/2-d_e} \partial_t(\rho_{f0} - \epsilon\beta_{\rho_f} T_{f1}) dy dx \\ + \frac{1}{\delta x} \int_{-(1/2-d_e)}^{1/2-d_e} \Big((\rho_{f0} q_0^{(1)} + \epsilon\rho_{f0} q_1^{(1)} - \epsilon\beta_{\rho_f} T_{f1} q_0^{(1)})|_{x=x_1+\delta_x} \\ - (\rho_{f0} q_0^{(1)} + \epsilon\rho_{f0} q_1^{(1)} - \epsilon\beta_{\rho_f} T_{f1} q_0^{(1)})|_{x=x_1} \Big) dy \\ + \frac{2}{\delta x} \int_{x_1}^{x_1+\delta x} (2\rho - (\rho_{f0} - \epsilon\beta_{\rho_f} T_{f1}))|_{y=-(1/2-d_e)} \partial_t d_e dx, \end{aligned}$$

where we have applied (22) in the last term. The notation $d_e = d_0 + \epsilon d_1$ is the effective grain width. The three integrals on the right-hand side are rewritten in different ways. In the first integral, the order of integration and differentiation is interchanged for the innermost integral. The second integral is rewritten using the effective transmissivity $\bar{q}_e = \int_{-(1/2-d_e)}^{1/2-d_e} q_e dy = \int_{-(1/2-d_e)}^{1/2-d_e} (q_0^{(1)} + \epsilon q_1^{(1)}) dy$ and the effective density $\rho_{fe} = \rho_{f0} - \epsilon\beta_{\rho_f} \bar{T}_{f1}$, where $\bar{T}_{f1} = \frac{1}{1-2d_e} \int_{-(1/2-d_e)}^{1/2-d_e} T_{f1} dy$. The

third integrand is rewritten by adding and subtracting a $\bar{T}_{f1}$-term in order to obtain an expression with ρ_{fe}. We then let δx approach zero, using the fundamental theorem in calculus and the definition of the derivative where applicable. Some terms cancel each other, hence we obtain

$$\partial_t\Big((1-2d_e)\rho_{fe}+2d_e2\rho\Big)+\partial_x(\rho_{fe}\bar{q}_e) \\ -\epsilon\beta_{\rho_f}\partial_x\Big(\int_{-(1/2-d_e)}^{1/2-d_e}T_{f1}q_0^{(1)}dy-\bar{T}_{f1}\bar{q}_0\Big)=O(\epsilon^2). \tag{35}$$

This equation will later serve as the upscaled mass conservation equation when the last term has been rewritten. From this equation we can also obtain the lowest order mass conservation equation by considering terms of $O(1)$ only. Then,

$$\partial_t\Big((1-2d_0)\rho_{f0}+2d_02\rho\Big)+\partial_x(\rho_{f0}\bar{q}_0)=0, \tag{36}$$

where $\bar{q}_0=\int_{-(1/2-d_0)}^{1/2-d_0}q_0^{(1)}dy$. This is the same equation as found in [7].

3.2 Conservation of momentum part I

We continue with the momentum equation and insert the required asymptotic expansion into (23). Recall that $q_0^{(2)}$ is equal to zero, hence

$$\begin{aligned}O(\epsilon^2)=&-\frac{1}{\epsilon}\partial_yp_0\mathbf{j}-\partial_xp_0\mathbf{i}-\partial_yp_1\mathbf{j}-\epsilon\partial_xp_1\mathbf{i}-\epsilon\partial_yp_2\mathbf{j}\\&+\mu_{f0}\partial_y^2q_0^{(1)}\mathbf{i}+\epsilon\mu_{f0}\partial_y^2q_1^{(1)}\mathbf{i}+\epsilon\mu_{f0}\partial_y^2q_1^{(2)}\mathbf{j}-\epsilon\beta_\mu\partial_y(T_{f1}\partial_yq_0^{(1)})\mathbf{i}+\epsilon\mu_{f0}\partial_y^2q_1^{(2)}\mathbf{j}\\&+\epsilon\partial_x(\mu_{f0}\partial_yq_0^{(1)})\mathbf{j}-\epsilon\frac{2}{3}\mu_{f0}\partial_y\partial_xq_0^{(1)}\mathbf{j}-\epsilon\frac{2}{3}\mu_{f0}\partial_y^2q_1^{(2)}\mathbf{j},\end{aligned}$$

where $\mu_{f0}=\mu_0-\beta_\mu T_{f0}$ is independent of y. The lowest order term is $\partial_yp_0=0$, which implies that $p_0=p_0(x,t)$. The horizontal and vertical component of the second lowest order terms are,

$$\begin{aligned}\partial_xp_0&=\mu_{f0}\partial_y^2q_0^{(1)},\\\partial_yp_1&=0.\end{aligned} \tag{37}$$

From the second equation we conclude $p_1=p_1(x,t)$. By making use of the horizontal component of the third lowest order terms, we obtain

$$\partial_xp_1=\mu_{f0}\partial_y^2q_1^{(1)}-\beta_\mu\partial_y(T_{f1}\partial_yq_0^{(1)})=0, \tag{38}$$

and then consider the sum of (37) and (38). Hence,

$$\partial_xp_0+\epsilon\partial_xp_1=\mu_{f0}\partial_y^2q_0^{(1)}+\epsilon\mu_{f0}\partial_y^2q_1^{(1)}-\epsilon\beta_\mu\partial_y(T_{f1}\partial_yq_0^{(1)})=0.$$

We introduce effective pressure $p_e=p_0+\epsilon p_1$, effective viscosity $\mu_{fe}=\mu_{f0}-\epsilon\beta_\mu\bar{T}_{f1}$ and effective horizontal velocity $q_e=q_0^{(1)}+\epsilon q_1^{(1)}$. Note that the two first are independent of y. Our equation hence reads

$$\partial_xp_e=\mu_{fe}\partial_y^2q_e-\epsilon\beta_\mu\partial_y\Big((T_{f1}-\bar{T}_{f1})\partial_yq_0^{(1)}\Big)+O(\epsilon^2). \tag{39}$$

To proceed, an explicit expression for $q_0^{(1)}$ must be found. The boundary condition for $q_0^{(1)}$ can be found from (34), hence $q_0^{(1)}=0$ at $y=\pm(1/2-d_0)$. We integrate (37) twice with respect to y, applying this boundary condition. Hence,

$$q_0^{(1)}=-\frac{1}{2}\frac{\partial_xp_0}{\mu_{f0}}\Big((\frac{1}{2}-d_0)^2-y^2\Big), \tag{40}$$

and we define the transmissivity $\bar{q}_0(x,t) = \int_{-(1/2-d_0)}^{1/2-d_0} q_0^{(1)}(x,y,t)dy$, which is

$$\bar{q}_0 = -\frac{2}{3}\frac{\partial_x p_0}{\mu_{f0}}(\frac{1}{2} - d_0)^3. \tag{41}$$

The boundary condition for q_e can also be found from (34), hence $q_e = 0$ at $y = \pm(1/2 - d_e)$. We insert (40) into (39), then integrate twice with respect to y and apply this boundary condition. This will result in

$$\begin{aligned}\frac{1}{2}\partial_x p_e\Big(y^2 - (\frac{1}{2} - d_e)^2\Big) &= \mu_{fe} q_e \\ &- \epsilon\frac{\beta_\mu}{\mu_{f0}}\partial_x p_0 \int_{-(1/2-d_e)}^{y} \Big(T_{f1}(x,z,t) - \bar{T}_{f1}(x,t)\Big) z dz + O(\epsilon^2).\end{aligned} \tag{42}$$

As with the mass conservation equation, the term involving T_{f1} needs to be rewritten. The effective transmissivity $\bar{q}_e$ can be found by integrating the above equation and will later serve as the upscaled Darcy's law with an additional Forchheimer-type term.

3.3 Conservation of ions

The effective ion concentration u_e is defined as

$$u_e = u_0 + \epsilon\bar{u}_1 = u_0 + \frac{\epsilon}{1-2d_e}\int_{-(1/2-d_e)}^{1/2-d_e} u_1 dy.$$

Later, we show that u_0 is independent of y, hence u_e will also be independent of y. The ion conservation equation (19) is integrated in y from $-(1/2 - d^\epsilon)$ to $1/2 - d^\epsilon$, resulting in

$$\begin{aligned}\int_{-(1/2-d^\epsilon)}^{1/2-d^\epsilon} \partial_t u^\epsilon dy + \int_{-(1/2-d^\epsilon)}^{1/2-d^\epsilon} \partial_x(u^\epsilon q^{\epsilon(1)})dy + \frac{1}{\epsilon}\int_{-(1/2-d^\epsilon)}^{1/2-d^\epsilon} \partial_y(u^\epsilon q^{\epsilon(2)})dy \\ = \epsilon D\int_{-(1/2-d^\epsilon)}^{1/2-d^\epsilon} \partial_x(\partial_x u^\epsilon)dy + \frac{1}{\epsilon}D\int_{-(1/2-d^\epsilon)}^{1/2-d^\epsilon} \partial_y(\partial_y u^\epsilon)dy.\end{aligned}$$

For the integrals of derivatives with respect to y, the integrals can be evaluated. For the remaining integrals, the order of integration and differentiation is interchanged, taking into account that the integration limits depend on x and t through d^ϵ. This will result in some terms to be evaluated at the boundary, to which we apply (20). Inserting asymptotic expansions and keeping terms up to $O(\epsilon^2)$ yield

$$\begin{aligned}\partial_t\Big(\int_{-(1/2-d_e)}^{1/2-d_e}(u_0 + \epsilon u_1)dy\Big) + 2\rho\partial_t d_e \\ +\partial_x\Big(\int_{-(1/2-d_e)}^{1/2-d_e}(u_0 + \epsilon u_1)(q_0^{(1)} + \epsilon q_1^{(1)})dy\Big) = \epsilon D\partial_x\Big(\int_{-(1/2-d_e)}^{1/2-d_e}\partial_x u_0 dy\Big) + O(\epsilon^2).\end{aligned}$$

By evaluating the integrals and rewriting,

$$\begin{aligned}\partial_t\Big((1-2d_e)u_e + 2d_e\rho\Big) + \partial_x(u_e\bar{q}_e) + \epsilon\partial_x\Big(\int_{-(1/2-d_e)}^{1/2-d_e} u_1 q_0^{(1)} dy - \bar{u}_1\bar{q}_0\Big) \\ = \epsilon D\partial_x\Big((1-2d_e)\partial_x u_e\Big) + O(\epsilon^2),\end{aligned} \tag{43}$$

is obtained.

It is necessary to express all terms using the effective variables, hence the last term on the first line in the above equation needs some extra care. We seek an explicit expression for u_1 and go back to the original conservation equation (19) and insert asymptotic expansions; hence,

$$\partial_t u_0 + \partial_x(u_0 q_0^{(1)}) + \partial_y(u_0 q_1^{(2)}) = \frac{1}{\epsilon}D\partial_y^2 u_0 + D\partial_y^2 u_1 + O(\epsilon).$$

The boundary condition (20) is

$$-D\partial_y u_0 - \epsilon D\partial_y u_1 - \epsilon\partial_x d_0 u_0 q_0^{(1)} + \epsilon u_0 q_1^{(2)} = -\epsilon(\rho - u_0)\partial_t d_0 + O(\epsilon^2).$$

The lowest order term is $\partial_y^2 u_0 = 0$, and the lowest order boundary condition is $\partial_y u_0 = 0$ at $y = \pm(1/2 - d_0)$. The only possibility is that $u_0 = u_0(x,t)$. Further, the second lowest order terms of the equation are

$$\partial_t u_0 + \partial_x(u_0 q_0^{(1)}) + \partial_y(u_0 q_1^{(2)}) = D\partial_y^2 u_1.$$

Rewriting using (33) enables us to write

$$\partial_t u_0 + q_0^{(1)}(\partial_x u_0 - \frac{u_0}{\rho_{f0}}\partial_x \rho_{f0}) - \frac{u_0}{\rho_{f0}}\partial_t \rho_{f0} = D\partial_y^2 u_1. \tag{44}$$

The second lowest order boundary condition is

$$D\partial_y u_1 = -\frac{u_0}{\rho_{f0}}(2\rho - \rho_{f0})\partial_t d_0 + (\rho - u_0)\partial_t d_0, \text{ at } y = -(1/2 - d_0), \tag{45}$$

where the boundary conditions for the velocity known from (34) are inserted.

We integrate (44) in y from $-(1/2 - d_e)$ to $1/2 - d_e$. We make some abuse of notation by writing $\bar{q}_0$ when applicable, which should only be used when the integral is from $-(1/2 - d_0)$ to $1/2 - d_0$. This abuse of notation introduces an error of $O(\epsilon)$ in (44), which in the final expression based on (43) will appear as an error of $O(\epsilon^2)$, which is tolerated. Hence,

$$(1 - 2d_e)\partial_t u_0 + \bar{q}_0(\partial_x u_0 - \frac{u_0}{\rho_{f0}\partial_x \rho_{f0}}) - (1 - 2d_e)\frac{u_0}{\rho_{f0}}\partial_t \rho_{f0} + 2D\partial_y u_1|_{y=-(1/2-d_e)} + O(\epsilon).$$

Multiplying (44) with $(1-2d_e)$ and subtracting from the above equation, and applying the boundary condition (45) at the same time, yield

$$\begin{aligned}(1 - 2d_e)D\partial_y^2 u_1 + (\partial_x u_0 - \frac{u_0}{\rho_{f0}}\partial_x \rho_{f0})\Big(\bar{q}_0 - (1 - 2d_e)q_0^{(1)}\Big) \\ -2\frac{u_0}{\rho_{f0}}(2\rho - \rho_{f0})\partial_t d_e + 2(\rho - u_0)\partial_t d_e = O(\epsilon).\end{aligned}$$

The expressions for $q_0^{(1)}$ and $\bar{q}_0$ known from (40) and (41) are inserted, and we introduce the shorthand notations $A(x,t) = (\partial_x u_0 - \frac{u_0}{\rho_{f0}}\partial_x \rho_{f0})\frac{\partial_x p_0}{\mu_{f0}}$ and $B(x,t) = -2\frac{u_0}{\rho_{f0}}(2\rho - \rho_{f0})\partial_t d_e + 2(\rho - u_0)\partial_t d_e$. By integrating in y from $-(1/2 - d_e)$ to y, and making use of the boundary condition (45), we obtain

$$2(\frac{1}{2} - d_e)D\partial_y u_1 + \frac{1}{3}A(\frac{1}{2} - d_e)\Big((\frac{1}{2} - d_e)^2 y - y^3\Big) + By = O(\epsilon).$$

Integrating once more from $-(1/2 - d_e)$ to y, results in

$$\begin{aligned}2(\frac{1}{2} - d_e)Du_1 - 2(\frac{1}{2} - d_e)Du_1|_{y=-(1/2-d_e)} \\ -\frac{1}{12}A(\frac{1}{2} - d_e)\Big(y^4 - 2(\frac{1}{2} - d_e)^2 y^2 + (\frac{1}{2} - d_e)^4\Big) + \frac{1}{2}B\Big(y^2 - (\frac{1}{2} - d_e)^2\Big) = O(\epsilon).\end{aligned}$$

Solving this equation for u_1 yields

$$\begin{aligned}u_1 = u_1|_{y=-(1/2-d_e)} + \frac{1}{24}\frac{A}{D}\Big(y^4 - 2(\frac{1}{2} - d_e)^2 y^2 + (\frac{1}{2} - d_e)^4\Big) \\ - \frac{1}{4}\frac{1}{1/2 - d_e}\frac{B}{D}\Big(y^2 - (\frac{1}{2} - d_e)^2\Big) + O(\epsilon),\end{aligned} \tag{46}$$

giving us an explicit expression for u_1 in terms of lower order functions. The expression is indeterminate due to the appearance of $u_1|_{y=-(1/2-d_e)}$ which we have no information about. However, this will not cause any difficulty as this term will cancel out in the resulting model equation.

In equation (43), we need to calculate $\int_{-(1/2-d_e)}^{1/2-d_e} u_1 q_0^{(1)} dy - \bar{u}_1 \bar{q}_0$. The first term is

$$\int_{-(1/2-d_e)}^{1/2-d_e} u_1 q_0^{(1)} dy = -u_1|_{y=-(1/2-d_e)} \frac{2}{3}\frac{\partial_x p_0}{\mu_0}(\frac{1}{2}-d_e)^3 - \frac{2}{105}\frac{A}{D}\frac{\partial_x p_0}{\mu_0}(\frac{1}{2}-d_e)^7 - \frac{2}{15}\frac{B}{D}\frac{\partial_x p_0}{\mu_0}(\frac{1}{2}-d_e)^4 + O(\epsilon).$$

For the second term, the average $\bar{u}_1$ is found to be

$$\begin{aligned}\bar{u}_1 &= \frac{1}{1-2d_e}\int_{-(1/2-d_e)}^{1/2-d_e} u_1 dy \\ &= u_1|_{y=-(1/2-d_e)} + \frac{1}{45}\frac{A}{D}(\frac{1}{2}-d_e)^4 + \frac{1}{6}\frac{B}{D}(\frac{1}{2}-d_e) + O(\epsilon). \end{aligned} \tag{47}$$

This means that the expression needed for (43) is

$$\begin{aligned}\int_{-(1/2-d_e)}^{1/2-d_e} u_1 q_0^{(1)} dy - \bar{u}_1\bar{q}_0 = &-\frac{1}{105}\frac{1}{D}(\frac{1}{2}-d_e)\bar{q}_0^2(\partial_x u_0 - \frac{u_0}{\rho_{f0}}\partial_x\rho_{f0}) \\ &+ \frac{1}{15}\frac{1}{D}(\frac{1}{2}-d_e)\bar{q}_0\Big((\rho-u_0)\partial_t d_e - \frac{u_0}{\rho_{f0}}(2\rho-\rho_{f0})\partial_t d_e\Big) + O(\epsilon).\end{aligned}$$

The resulting equation for the effective concentration u_e is then

$$\begin{aligned}&\partial_t\Big((1-2d_e)u_e + 2d_e\rho\Big) + \partial_x(u_e\bar{q}_e) \\ &\quad= \epsilon D\partial_x\Big((1-2d_e)\partial_x u_e(1+\frac{\bar{q}_e^2}{210D^2}) - (1-2d_e)\frac{\bar{q}_e^2}{210D^2}\frac{u_e}{\rho_{fe}}\partial_x\rho_{fe} \\ &\quad+ (1-2d_e)\frac{\bar{q}_e}{60D^2}\partial_t(2d_e)\big(\frac{u_e}{\rho_{fe}}(2\rho-\rho_{fe}) - (\rho-u_e)\big)\Big) + O(\epsilon^2).\end{aligned}$$

3.4 Conservation of energy

We define effective fluid temperature and effective grain temperature:

$$\begin{aligned}T_{fe} &= T_{f0} + \epsilon\bar{T}_{f1} = T_{f0} + \frac{\epsilon}{1-2d_e}\int_{-(1/2-d_e)}^{1/2-d_e} T_{f1}dy, \\ T_{ge} &= T_{g0} + \epsilon\bar{T}_{g1} = T_{g0} + \frac{\epsilon}{d_e}\int_{-1/2}^{-(1/2-d_e)} T_{g1}dy.\end{aligned}$$

Soon, we show that T_{f0} and T_{g0} are independent of y and in fact equal due to the continuity condition (28). In general, $\bar{T}_{f1}$ and $\bar{T}_{g1}$ will not be equal. The conservation equations (25) and (26) are integrated over their respective domains in y and summed, resulting in

$$\begin{aligned}&\int_{-(1/2-d^\epsilon)}^{1/2-d^\epsilon}\partial_t(\rho_f T_f^\epsilon)dy + 2\int_{-1/2}^{-(1/2-d^\epsilon)}\partial_t(\varsigma\rho T_g^\epsilon)dy \\ &\quad+\int_{-(1/2-d^\epsilon)}^{1/2-d^\epsilon}\partial_x(\rho_f T_f^\epsilon q^{\epsilon(1)})dy + \frac{1}{\epsilon}\int_{-(1/2-d^\epsilon)}^{1/2-d^\epsilon}\partial_y(\rho_f T_f^\epsilon q^{\epsilon(2)})dy \\ &\quad=\epsilon\int_{-(1/2-d^\epsilon)}^{1/2-d^\epsilon}\partial_x(\kappa_f\partial_x T_f^\epsilon)dy + \frac{1}{\epsilon}\int_{-(1/2-d^\epsilon)}^{1/2-d^\epsilon}\partial_y(\kappa_f\partial_y T_f^\epsilon)dy \\ &\quad+2\epsilon\int_{-1/2}^{-(1/2-d^\epsilon)}\partial_x(\kappa_g\partial_x T_g^\epsilon)dy + \frac{2}{\epsilon}\int_{-1/2}^{-(1/2-d^\epsilon)}\partial_y(\kappa_g\partial_y T_g^\epsilon)dy.\end{aligned}$$

The integrals of derivatives of y are evaluated, while in the remaining integrals we interchange the order of integration and differentiation. Applying the boundary condition (27) causes the terms evaluated at $y = -(1/2 - d^\epsilon)$ to cancel out. We insert the necessary asymptotic expansions, hence

$$\begin{aligned}
&\partial_t\Big(\int_{-(1/2-d_e)}^{1/2-d_e}(\rho_{f0}-\epsilon\beta_{\rho_f}T_{f1})(T_{f0}+\epsilon T_{f1})dy\Big)+2\partial_t\Big(\int_{-1/2}^{-(1/2-d_e)}\varsigma\rho(T_{g0}+\epsilon T_{g1})dy\Big)\\
&\quad+\partial_x\Big(\int_{-(1/2-d_e)}^{1/2-d_e}(\rho_{f0}-\epsilon\beta_{\rho_f}T_{f1})(T_{f0}+\epsilon T_{f1})(q_0^{(1)}+\epsilon q_1^{(1)})dy\Big)\\
&\quad=\epsilon\partial_x\Big(\int_{-(1/2-d_e)}^{1/2-d_e}\kappa_f\partial_x T_{f0}dy\Big)+2\epsilon\partial_x\Big(\int_{-1/2}^{-(1/2-d_e)}\kappa_g\partial_x T_{g0}dy\Big)+O(\epsilon^2).
\end{aligned}$$

Using that ρ_{f0}, T_{f0} and T_{g0} are independent of y, this can be written as

$$\begin{aligned}
&\partial_t\Big((1-2d_e)\rho_{fe}T_{fe}+2d_e\varsigma\rho T_{ge}\Big)+\partial_x(\rho_{fe}T_{fe}\bar{q}_e)\\
&\quad+\epsilon\partial_x\Big((\rho_{f0}-\beta_{\rho_f}T_{f0})\big\{\int_{-(1/2-d_e)}^{1/2-d_e}T_{f1}q_0^{(1)}dy-\bar{T}_{f1}\bar{q}_0\big\}\Big)\\
&\quad=\epsilon\partial_x\Big((1-2d_e)\kappa_f\partial_x T_{fe}+2d_e\kappa_g\partial_x T_{ge}\Big)+O(\epsilon^2). \qquad (48)
\end{aligned}$$

The T_{f1}-part needs to be rewritten. Also, since there is one equation and two unknowns T_{fe} and T_{ge}, one more equation in needed to have a consistent formulation. Both of these difficulties are solved by finding explicit expressions for T_{f1} and T_{g1}, using a similar technique as performed for u_1.

The necessary asymptotic expansions are inserted into (25), (26), (27), (28) and (29), keeping the lowest order terms. The energy equations are then

$$\begin{aligned}
&\partial_t(\rho_{f0}T_{f0})+\partial_x(\rho_{f0}T_{f0}q_0^{(1)})+\partial_y(\rho_{f0}T_{f0}q_1^{(2)})=\frac{1}{\epsilon}\partial_y\Big(\kappa_f\partial_y(T_{f0}+\epsilon T_{f1})\Big)+O(\epsilon);\\
&\partial_t(\varsigma\rho T_{g0})=\frac{1}{\epsilon}\partial_y\Big(\kappa_g\partial_y(T_{g0}+\epsilon T_{g1})\Big)+O(\epsilon),
\end{aligned}$$

while the boundary conditions for the lower part of the moving boundary are

$$\begin{aligned}
-\kappa_f\partial_y T_{f0}-\epsilon\kappa_f\partial_y T_{f1}+\epsilon\rho_{f0}q_1^{(2)}T_{f0}+\kappa_g\partial_y T_{g0}+\epsilon\kappa_g\partial_y T_{g1}&\\
=-\epsilon(\varsigma\rho T_{g0}-\rho_{f0}T_{f0})\partial_t d_0+O(\epsilon^2);&\\
T_{f0}+\epsilon T_{f1}=T_{g0}+\epsilon T_{g1}+O(\epsilon^2),&
\end{aligned}$$

and the boundary condition at the top and bottom of the strip is

$$\partial_y T_{g0}+\epsilon\partial_y T_{g1}=O(\epsilon^2).$$

Collecting the lowest order terms from the five above equations, results in the system

$$\begin{aligned}
\partial_y^2 T_{f0}&=0 && \text{for } -(1/2-d_0)\le y\le 1/2-d_0,\\
\partial_y^2 T_{g0}&=0 && \text{for } 1/2-d_0\le|y|\le 1/2,\\
\kappa_f\partial_y T_{f0}&=\kappa_g\partial_y T_{g0} && \text{at } y=\pm(1/2-d_0),\\
T_{f0}&=T_{g0} && \text{at } y=\pm(1/2-d_0),\\
\partial_y T_{g0}&=0 && \text{at } y=\pm 1/2.
\end{aligned}$$

The only possible solution is that T_{f0} and T_{g0} are equal and independent of y, hence $T_0(x,t) = T_{f0}(x,t) = T_{g0}(x,t)$ can be defined. Next step is to consider the $O(1)$-parts of the energy equations independently.

The $O(1)$-part of the void space energy equation is

$$\partial_t(\rho_{f0}T_{f0}) + \partial_x(\rho_{f0}T_{f0}q_0^{(1)}) + \partial_y(\rho_{f0}T_{f0}q_1^{(2)}) = \kappa_f\partial_y^2 T_{f1}.$$

Using (33) to eliminate $q_1^{(2)}$, this can be written

$$\rho_{f0}\partial_t T_{f0} + \rho_{f0}q_0^{(1)}\partial_x T_{f0} = \kappa_f\partial_y^2 T_{f1}. \tag{49}$$

Integrating in y from $-(1/2-d_e)$ to $(1/2-d_e)$ gives us

$$(1-2d_e)\rho_{f0}\partial_t T_{f0} + \rho_{f0}\partial_x T_{f0}\bar{q}_0 = -2\kappa_f\partial_y T_{f1}|_{y=-(1/2-d_e)} + O(\epsilon), \tag{50}$$

which can also serve as a boundary condition for $\partial_y T_{f1}$ at $y=-(1/2-d_e)$. Multiplying (49) with $(1-2d_e)$ and subtracting from (50) result in

$$(1-2d_e)\kappa_f\partial_y^2 T_{f1} = \rho_{f0}\partial_x T_{f0}\Big((1-2d_e)q_0^{(1)} - \bar{q}_0\Big) - 2\kappa_f\partial_y T_{f1}|_{y=-(1/2-d_e)} + O(\epsilon).$$

To ease the notation, we do not insert the boundary condition for $\partial_y T_{f1}$ at $y=-(1/2-d_e)$ at this moment. We do however insert the expressions for the velocities known from (40) and (41), hence

$$2(\frac{1}{2}-d_e)\kappa_f\partial_y^2 T_{f1} = C(x,t)(\frac{1}{2}-d_e)\Big(y^2 - \frac{1}{3}(\frac{1}{2}-d_e)^2\Big) - 2\kappa_f\partial_y T_{f1}|_{y=-(1/2-d_e)} + O(\epsilon),$$

where $C(x,t) = \rho_{f0}\partial_x T_{f0}\frac{\partial_x p_0}{\mu_{f0}}$. Integrating twice in y from $-(1/2-d_e)$ to y, results in

$$\begin{aligned}
2(\frac{1}{2}-d_e)\kappa_f T_{f1} = {} & 2(\frac{1}{2}-d_e)\kappa_f T_{f1}|_{y=-(1/2-d_e)} \\
& + \frac{1}{12}C(x,t)(\frac{1}{2}-d_e)\Big(y^4 - 2(\frac{1}{2}-d_e)^2y^2 + (\frac{1}{2}-d_e)^4\Big) \\
& - \kappa_f\partial_y T_{f1}|_{y=-(1/2-d_e)}\Big(y^2 - (\frac{1}{2}-d_e)^2\Big) + O(\epsilon),
\end{aligned}$$

which means that

$$\begin{aligned}
T_{f1} = {} & T_{f1}|_{y=-(1/2-d_e)} + \frac{1}{24}\frac{C}{\kappa_f}\Big(y^4 - 2(\frac{1}{2}-d_e)^2y^2 + (\frac{1}{2}-d_e)^4\Big) \\
& - \frac{1}{2}\frac{1}{1/2-d_e}\partial_y T_{f1}|_{y=-(1/2-d_e)}\Big(y^2 - (\frac{1}{2}-d_e)^2\Big) + O(\epsilon).
\end{aligned} \tag{51}$$

The average $\bar{T}_{f1}$ is then

$$\bar{T}_{f1} = T_{f1}|_{y=-(1/2-d_e)} + \frac{1}{45}\frac{C}{\kappa_f}(\frac{1}{2}-d_e)^4 + \frac{1}{3}\partial_y T_{f1}|_{y=-(1/2-d_e)}(\frac{1}{2}-d_e) + O(\epsilon). \tag{52}$$

We turn our attention to the $O(1)$ terms from the grain space energy equation:

$$\partial_t(\varsigma\rho T_{g0}) = \kappa_g\partial_y^2 T_{g1}.$$

Integrating in y from $-1/2$ to $-(1/2-d_e)$ gives us

$$d_e\partial_t(\varsigma\rho T_{g0}) = \kappa_g\partial_y T_{g1}|_{y=-(1/2-d_e)}, \tag{53}$$

which later can be used as a boundary condition for $\partial_y T_{g1}$ at $y=-(1/2-d_e)$. Next step is to multiply the $O(1)$ terms with d_e and subtract from the above equation, resulting in

$$d_e\kappa_g\partial_y^2 T_{g1} = \kappa_g\partial_y T_{g1}|_{y=-(1/2-d_e)}.$$

This equation is integrated first from $-1/2$ to y, then from y to $-(1/2-d_e)$, giving us

$$T_{g1} = T_{g1}|_{y=-(1/2-d_e)} + \frac{1}{2d_e}\partial_y T_{g1}|_{y=-(1/2-d_e)}\Big(y^2 + y + (\frac{1}{2}-d_e) - (\frac{1}{2}-d_e)^2\Big) + O(\epsilon).$$

The average is

$$\bar{T}_{g1} = T_{g1}|_{y=-(1/2-d_e)} - \frac{1}{3}d_e\partial_y T_{g1}|_{y=-(1/2-d_e)} + O(\epsilon).$$

The expressions for T_{f1} and T_{g1} and their averages involves the function evaluation of T_{f1} and T_{g1} at $y=-(1/2-d_e)$. Due to the boundary condition (28) these are known to be equal, even though we do not know the value. As $T_{fe} = T_0 + \epsilon\bar{T}_{f1}$ and $T_{ge} = T_0 + \epsilon\bar{T}_{g1}$, we can calculate the difference

$$\begin{aligned} T_{fe} - T_{ge} = \epsilon\Big\{ &\frac{2d_e}{12}(\frac{1-2d_e}{\kappa_f} + \frac{2d_e}{\kappa_g})\partial_t(\varsigma\rho T_{ge}) \\ &+ \frac{1}{12}\frac{1}{\kappa_f}(1-2d_e)\Big((\varsigma\rho T_{ge} - \rho_{fe}T_{fe}) - T_{fe}(2\rho - f\rho_{fe})\Big)\partial_t(2d_e) \\ &- \frac{1}{60}\frac{1}{\kappa_f}(1-2d_e)\rho_{fe}\partial_x T_{fe}\bar{q}_e\Big\} + O(\epsilon^2), \end{aligned}$$

where we have rewritten using (35) and (48) and inserted the boundary conditions for $\partial_y T_{f1}$ and $\partial_y T_{g1}$ at $y=-(1/2-d_e)$. This equation will be a part of the final set of equations and acts as the second relation between the variables T_{fe} and T_{ge}.

To find the required T_{f1}-expression in equation (48), we calculate

$$\begin{aligned} \int_{-(1/2-d_e)}^{1/2-d_e} T_{f1}q_0^{(1)}dy - \bar{T}_{f1}\bar{q}_0 = &\frac{1}{60}\frac{1}{\kappa_f}(1-2d_e)\bar{q}_e\Big(2d_e\partial_t(\varsigma\rho T_{ge}) \\ &+ (\varsigma\rho T_{ge} - \rho_{fe}T_{fe})\partial_t(2d_e) - T_{fe}(2\rho - \rho_{fe})\partial_t(2d_e)\Big) \\ &- \frac{1}{210}\frac{1}{\kappa_f}(1-2d_e)\rho_{fe}\partial_x T_{fe}\bar{q}_e^2 + O(\epsilon). \end{aligned} \tag{54}$$

Inserting this into (48), results in

$$\begin{aligned} &\partial_t\Big((1-2d_e)\rho_{fe}T_{fe} + 2d_e\varsigma\rho T_{ge}\Big) + \partial_x(\rho_{fe}T_{fe}\bar{q}_e) \\ &=\epsilon\kappa_f\partial_x\Big\{(1-2d_e)\partial_x T_{fe}\Big(1 + \frac{\bar{q}_e^2}{210\kappa_f^2}\rho_{fe}(\rho_{fe} - \beta_{\rho_f}T_{fe})\Big) \\ &-\frac{\bar{q}_e}{60\kappa_f^2}(1-2d_e)(\rho_{fe} - \beta_{\rho_f}T_{fe})\Big(2d_e\partial_t(\varsigma\rho T_{ge}) + (\varsigma\rho T_{ge} \\ &\quad - \rho_{fe}T_{fe})\partial_t(2d_e) - T_{fe}(2\rho - \rho_{fe})\partial_t(2d_e)\Big)\Big\} + \epsilon\kappa_g\partial_x(2d_e\partial_x T_{ge}) + O(\epsilon^2). \end{aligned}$$

3.5 Conservation of mass part II

We turn back to equation (35), where inserting (54) results in

$$\begin{aligned} \partial_t\Big((1-2d_e)\rho_{fe} + 2d_e 2\rho\Big) + \partial_x(\rho_{fe}\bar{q}_e) = \epsilon\frac{\beta}{\kappa_f}\partial_x\Big\{ &-\frac{\bar{q}_e^2}{210}(1-2d_e)\rho_{fe}\partial_x T_{fe} \\ &+\frac{\bar{q}_e}{60}(1-2d_e)\Big(2d_e\partial_t(\varsigma\rho T_{ge}) + (\varsigma\rho T_{ge} - \rho_{fe}T_{fe})\partial_t(2d_e) \\ &- T_{fe}(2\rho - \rho_{fe})\partial_t(2d_e)\Big)\Big\} + O(\epsilon^2). \end{aligned}$$

3.6 Conservation of momentum part II

Inserting (51) and (52) into (42) and evaluating the integral yield

$$\begin{aligned}\frac{1}{2}\partial_x p_e\Big(y^2-(\frac{1}{2}-d_e)^2\Big) &= \mu_{fe}q_e\\ -\epsilon\frac{\beta_\mu}{\mu_{f0}}\partial_x p_0\Big(\frac{1}{24}\frac{C}{\kappa_f}\big(\frac{1}{6}y^6-\frac{1}{2}(\frac{1}{2}-d_e)^2y^4+\frac{7}{30}(\frac{1}{2}-d_e)^4y^2+\frac{1}{10}(\frac{1}{2}-d_e)^6\big)\\ +\frac{1}{2}\frac{1}{\frac{1}{2}-d_e}\partial_y T_{f1}|_{y=-(1/2-d_e)}\big(-\frac{1}{4}y^4+\frac{1}{6}(\frac{1}{2}-d_e)^2y^2+\frac{1}{12}(\frac{1}{2}-d_e)^4\big)\Big)+O(\epsilon^2).\end{aligned}$$

Integrating this equation in y to obtain an expression involving $\bar{q}_e$, yields

$$\begin{aligned}-\frac{2}{3}\partial_x p_e(\frac{1}{2}-d_e)^3 &= \mu_{fe}\bar{q}_e\\ -\epsilon\frac{\beta_\mu\rho_{f0}}{\mu_{f0}\kappa_f}\partial_x p_0\Big(\frac{4}{105}\partial_x T_{f0}\frac{\partial_x p_0}{\mu_{f0}}(\frac{1}{2}-d_e)^7-\frac{4}{45}\partial_t T_{f0}(\frac{1}{2}-d_e)^5\Big)+O(\epsilon^2).\end{aligned}$$

This equation can be rewritten in two different ways. We can either solve the above equation for $\bar{q}_e$, or we can use (40) to rewrite the factors involving $\partial_x p_0$ to get an expression showing the relation to the Forchheimer-form of Darcy's law. Hence, the above equation can be written either as

$$\begin{aligned}\bar{q}_e=-\frac{(1-2d_e)^3}{12\mu_{fe}}\partial_x p_e\Big(1-\epsilon\frac{\beta_\mu\rho_{fe}}{\mu_{fe}\kappa_f}(1-2d_e)^2\big(-\frac{1}{30}\partial_t T_{fe}\\ +\frac{1}{280}\partial_x T_{fe}\frac{\partial_x p_e}{\mu_{fe}}(1-2d_e)^2\big)\Big)+O(\epsilon^2),\end{aligned}$$

or as

$$\begin{aligned}\partial_x p_e =&-\bar{q}_e\frac{12\mu_{fe}}{(1-2d_e)^3}\Big(1-\epsilon\frac{\beta_\mu\rho_{fe}}{\mu_{fe}\kappa_f}\frac{1}{30}\partial_t T_{fe}(1-2d_e)^2\Big)\\ &+\epsilon\bar{q}_e^2\frac{12\rho_{fe}}{(1-2d_e)^3}\frac{\beta_\mu}{\kappa_f}\frac{3}{70}\partial_x T_{fe}(1-2d_e)+O(\epsilon^2).\end{aligned}$$

As an error of $O(\epsilon^2)$ is made in both cases, the two forms are equivalent. Further, this also justifies replacing μ_{f0} by μ_{fe}. Note that the non-linear term in Forchheimer's Law is a negative term, while we have a term that could be either positive or negative depending on the sign of $\partial_x T_{fe}$. The Forchheimer's law is due to inertial effects under different assumptions than considered here, but is similar to ours in the sense of introducing a non-linearity in the flow equation when considering a large Péclet number. Our non-linear term is a secondary effect due to the varying viscosity and dominating convection. As a fluid with varying viscosity is transported through the pore, non-linear inertial effects appear, which is indicated by the non-linear term containing the factors β_μ and $\partial_x T_{fe}$. Since the viscosity can either increase or decrease, the sign of the non-linear term varies with the sign of the temperature change. We note that for most fluids and temperature ranges the viscosity changes will not be large, hence the value of β_μ, and accordingly the non-linearity, will be small.

3.7 How reactions affect the varying aperture

To upscale (30), we first need to regularize the dissolution rate (31) to obtain a Lipschitz continuous function. We define $f_\delta(T_f^\epsilon, d^\epsilon) = k_0 e^{-\alpha/T_f^\epsilon} w_\delta(d^\epsilon)$ where

$$w_\delta(d^\epsilon)=\begin{cases}0 & \text{if } d^\epsilon<0,\\ d^\epsilon/\delta & \text{if } 0\le d^\epsilon<\delta,\\ 1 & \text{if } d^\epsilon\ge\delta,\end{cases}\tag{55}$$

for some small $\delta > 0$. Inserting asymptotic expansions into (30) yields

$$\partial_t(\rho d_e) = \Big(f_p(T_{f0} + \epsilon T_{f1} + O(\epsilon^2), u_0 + \epsilon u_1 + O(\epsilon^2)) \\ - f_\delta(T_{f0} + \epsilon T_{f1} + O(\epsilon^2), d_e + O(\epsilon^2))\Big) + O(\epsilon^2),$$

where the functions depending on y should be evaluated at $y = -(1/2 - d_e)$. We Taylor expand the precipitation rate around (T_{fe}, u_e), and the dissolution rate around (T_{fe}, d_e). Hence,

$$\partial_t(\rho d_e) = \Big(f_p(T_{fe}, u_e) + \epsilon\partial_1 f_p(T_{f1}|_{y=-(1/2-d_e)} - \bar{T}_{f1}) + \epsilon\partial_2 f_p(u_1|_{y=-(1/2-d_e)} - \bar{u}_1)\Big) \\ - \Big(f_\delta(T_{fe}, d_e) + \epsilon\partial_1 f_\delta(T_{f1}|_{y=-(1/2-d_e)} - \bar{T}_{f1})\Big) + O(\epsilon^2).$$

Letting δ approach zero, gives the original $w(d_e, T_{fe}, u_e)$. Since $\bar{u}_1$ and $\bar{T}_{f1}$ are known from (47) and (52), we obtain

$$\partial_t(\rho d_e) = f_p(T_{fe}, u_e) - f_d(T_{fe}, u_e d_e) + \epsilon\Big\{(\partial_1 f_p - \partial_1 f_d)\Big(\frac{1}{60}\frac{1}{\kappa_f}(1-2d_e)\rho_{fe}\partial_x T_{fe}\bar{q}_e \\ -\frac{1}{12}\frac{1}{\kappa_f}(1-2d_e)\big(2d_e\partial_t(\varsigma\rho T_{ge}) + (\varsigma\rho T_{ge} - \rho_{fe}T_{fe})\partial_t(2d_e) \\ - T_{fe}(2\rho - \rho_{fe})\partial_t(2d_e)\big)\Big) + \partial_2 f_p\Big(\frac{1}{60}\frac{1}{D}(1-2d_e)(\partial_x u_e - \frac{u_e}{\rho_{fe}}\partial_x\rho_{fe})\bar{q}_e \\ -\frac{1}{12}\frac{1}{D}(1-2d_e)\big((\rho - u_e) - \frac{u_e}{\rho_{fe}}(2\rho - \rho_{fe})\big)\partial_t(2d_e)\Big)\Big\} + O(\epsilon^2).$$

3.8 Upscaled equations

We now summarize the upscaled equations. There are six unknowns: $u_e(x,t)$, $\bar{q}_e(x,t)$, $d_e(x,t)$, $p_e(x,t)$, $T_{fe}(x,t)$ and $T_{ge}(x,t)$, and six equations to describe them. Note that all the variables depend only on x and t, hence our thin strip model has reduced to a one-dimensional problem. The governing system of equations is defined for $0 \le x \le 1$ and for $t > 0$, and is given by

$$\bar{q}_e = -\frac{(1-2d_e)^3}{12\mu_{fe}}\partial_x p_e\Big\{1 - \epsilon\frac{\beta_\mu\rho_{fe}}{\mu_{fe}\kappa_f}(1-2d_e)^2\big(-\frac{1}{30}\partial_t T_{fe} \\ + \frac{1}{280}\partial_x T_{fe}\frac{\partial_x p_e}{\mu_{fe}}(1-2d_e)^2\big)\Big\}; \tag{56}$$

$$\partial_t\Big((1-2d_e)\rho_{fe} + 2d_e 2\rho\Big) + \partial_x(\rho_{fe}\bar{q}_e) = \epsilon\frac{\beta}{\kappa_f}\partial_x\Big\{-\frac{\bar{q}_e^2}{210}(1-2d_e)\rho_{fe}\partial_x T_{fe} \\ + \frac{\bar{q}_e}{60}(1-2d_e)\Big(2d_e\partial_t(\varsigma\rho T_{ge}) + (\varsigma\rho T_{ge} - \rho_{fe}T_{fe})\partial_t(2d_e) \\ - T_{fe}(2\rho - \rho_{fe})\partial_t(2d_e)\Big)\Big\}; \tag{57}$$

$$\partial_t(\rho d_e) = f_p(T_{fe}, u_e) - f_d(T_{fe}, d_e) + \epsilon\Big\{(\partial_1 f_p - \partial_1 f_d)\Big(\frac{1}{60}\frac{1}{\kappa_f}(1-2d_e)\rho_{fe}\partial_x T_{fe}\bar{q}_e \\ -\frac{1}{12}\frac{1}{\kappa_f}(1-2d_e)\big(2d_e\partial_t(\varsigma\rho T_{ge}) + (\varsigma\rho T_{ge} - \rho_{fe}T_{fe})\partial_t(2d_e) \\ - T_{fe}(2\rho - \rho_{fe})\partial_t(2d_e)\big)\Big) + \partial_2 f_p\Big(\frac{1}{60}\frac{1}{D}(1-2d_e)(\partial_x u_e - \frac{u_e}{\rho_{fe}}\partial_x\rho_{fe})\bar{q}_e \\ -\frac{1}{12}\frac{1}{D}(1-2d_e)\big((\rho - u_e) - \frac{u_e}{\rho_{fe}}(2\rho - \rho_{fe})\big)\partial_t(2d_e)\Big)\Big\}; \tag{58}$$

$$\partial_t\Big((1-2d_e)u_e+2d_e\rho\Big)+\partial_x(u_e\bar{q}_e)$$
$$=\epsilon D\partial_x\Big((1-2d_e)\partial_x u_e(1+\frac{\bar{q}_e^2}{210D^2})-(1-2d_e)\frac{\bar{q}_e^2}{210D^2}\frac{u_e}{\rho_{fe}}\partial_x\rho_{fe}$$
$$-(1-2d_e)\frac{\bar{q}_e}{60D^2}\partial_t(2d_e)\big((\rho-u_e)-\frac{u_e}{\rho_{fe}}(2\rho-\rho_{fe})\big)\Big); \tag{59}$$

$$\partial_t\Big((1-2d_e)\rho_{fe}T_{fe}+2d_e\varsigma\rho T_{ge}\Big)+\partial_x(\rho_{fe}T_{fe}\bar{q}_e)$$
$$=\epsilon\kappa_f\partial_x\Big\{(1-2d_e)\partial_x T_{fe}\Big(1+\frac{\bar{q}_e^2}{210\kappa_f^2}\rho_{fe}(\rho_{fe}-\beta_{\rho_f}T_{fe})\Big)$$
$$-\frac{\bar{q}_e}{60\kappa_f^2}(1-2d_e)(\rho_{fe}-\beta_{\rho_f}T_{fe})\Big(2d_e\partial_t(\varsigma\rho T_{ge})+(\varsigma\rho T_{ge}-\rho_{fe}T_{fe})\partial_t(2d_e)$$
$$-T_{fe}(2\rho-\rho_{fe})\partial_t(2d_e)\Big)\Big\}+\epsilon\kappa_g\partial_x(2d_e\partial_x T_{ge}); \tag{60}$$

$$T_{fe}-T_{ge}=\epsilon\Big\{\frac{2d_e}{12}(\frac{1-2d_e}{\kappa_f}+\frac{2d_e}{\kappa_g})\partial_t(\varsigma\rho T_{ge})-\frac{1}{60}\frac{1}{\kappa_f}(1-2d_e)\rho_{fe}\partial_x T_{fe}\bar{q}_e$$
$$+\frac{1}{12}\frac{1}{\kappa_f}(1-2d_e)\Big((\varsigma\rho T_{ge}-\rho_{fe}T_{fe})-T_{fe}(2\rho-f\rho_{fe})\Big)\partial_t(2d_e)\Big\}. \tag{61}$$

where terms of $O(\epsilon^2)$ have been neglected. The fluid density and viscosity are given by

$$\rho_{fe}=\rho_{fe}(T_{fe})=\rho_0-\beta_{\rho_f}T_{fe} \text{ and } \mu_{fe}=\mu_{fe}(T_{fe})=\mu_0-\beta_\mu T_{fe}. \tag{62}$$

Dispersive terms are found in several of the model equations. The model equations also contain correction terms of $O(\epsilon)$ that are due to the changing geometry, e.g. $(\varsigma\rho T_{ge}-\rho_{fe}T_{fe})\partial_t(2d_e)$ in (60). The difference is the jump in the effective energy across the moving boundary.

Compared to the dispersive model studied by Kumar et al in [15], our system of equations is more coupled due to the reaction rates and the fluid density depending on temperature. Also, the model in [15] does not take into account volume change due to chemical reactions, which in our model can be found in terms including a $(2\rho-\rho_{fe})$-factor. As Kumar et al assume constant fluid density and that $2\rho=\rho_f$, their model lacks terms with derivatives of ρ_{fe} and the $(2\rho-\rho_{fe})$-factor which can be found in the present work. Since we also take into account varying viscosity, an extra non-linear term in Darcy's law appears. This term can be interpreted as a Forchheimer-type term, which appears when inertial effects on the flow are important; see, e.g., [12] for derivation of the Forchheimer Law in the isothermal case. Note that the Forchheimer's law is derived under different assumptions than considered here, but the present flow equation shows similarities due to the non-isothermal effects arising from the viscosity.

Compared to our previous work in [7], one large difference is the need of an extra equation to describe the temperature. In [7] it was only necessary to use the lowest order temperature T_0, while in the present work we have to include the average of the first order correction terms, which are not necessarily equal. The last equation in the above system is expressing how the two effective temperatures T_{fe} and T_{ge} deviate from each other. Note that the deviations are of $O(\epsilon)$.

4 Numerical results

We consider two types of comparisons: First, we compare the upscaled model with two simpler versions still honoring the varying geometry; a model obtained by simple upscaling where diffusion is included, and an hyperbolic model obtained by removing all terms of order ϵ. Secondly, we compare the upscaled model with one obtained using a fixed geometry. The goal of these comparisons is to emphasize similarities and differences between the various models and provide some guidelines for when it is necessary to use a complicated model, and when it can be replaced by a simpler version.

4.1 Comparison with two simpler models

In the following, the upscaled model (56)-(61) will be called the dispersive model.

A simple upscaling where diffusive terms, but no other $O(\epsilon)$-terms, are included, results in a model similar as the one in [7]. This model will include five unknowns u_e, $\bar{q}_e$, d_e, p_e and T_e and five equations to describe them and will be called the simple upscaled model throughout the comparison. The variables are denoted with subscript e for consistency with the notation in the dispersive model. All equations are defined for $0 \leq x \leq 1$, $t > 0$, and are given by

$$\bar{q}_e = -\frac{(1-2d_e)^3}{12\mu_{fe}}\partial_x p_e; \tag{63}$$

$$\partial_t\Big((1-2d_e)\rho_{fe} + 2d_e 2\rho\Big) + \partial_x(\rho_{fe}\bar{q}_e) = 0; \tag{64}$$

$$\partial_t(\rho d_e) = f_p(T_e, u_e) - f_d(T_e, d_e); \tag{65}$$

$$\partial_t\Big((1-2d_e)u_e + 2d_e\rho\Big) + \partial_x(u_e\bar{q}_e) = \epsilon D\partial_x\Big((1-2d_e)\partial_x u_e\Big); \tag{66}$$

$$\begin{aligned}\partial_t\Big((1-2d_e)\rho_{fe}T_e + 2d_e\varsigma\rho T_e\Big) + \partial_x(\rho_{fe}T_e\bar{q}_e) =& \epsilon\kappa_f\partial_x\Big((1-2d_e)\partial_x T_e\Big) \\ &+\epsilon\kappa_g\partial_x\Big(2d_e\partial_x T_e\Big),\end{aligned} \tag{67}$$

together with (62) for fluid density and viscosity.

By doing a straightforward upscaling of the model equations, only keeping leading order terms, an hyperbolic model is obtained. This model will include five unknowns u_e, $\bar{q}_e$, d_e, p_e and T_e and five equations to describe them. All equations are defined for $0 \leq x \leq 1$, $t > 0$, and are given by

$$\bar{q}_e = -\frac{(1-2d_e)^3}{12\mu_{fe}}\partial_x p_e; \tag{68}$$

$$\partial_t\Big((1-2d_e)\rho_{fe} + 2d_e 2\rho\Big) + \partial_x(\rho_{fe}\bar{q}_e) = 0; \tag{69}$$

$$\partial_t(\rho d_e) = f_p(T_e, u_e) - f_d(T_e, d_e); \tag{70}$$

$$\partial_t\Big((1-2d_e)u_e + 2d_e\rho\Big) + \partial_x(u_e\bar{q}_e) = 0; \tag{71}$$

$$\partial_t\Big((1-2d_e)\rho_{fe}T_e + 2d_e\varsigma\rho T_e\Big) + \partial_x(\rho_{fe}T_e\bar{q}_e) = 0, \tag{72}$$

together with (62) for fluid density and viscosity.

The simple upscaled model (63)-(67) and the hyperbolic model (68)-(72) still honor the varying grain width and include the same couplings with respect to non-isothermal effects and assumptions on large Péclet number as in the dispersive model (56)-(61). However, these two simpler versions differ from the dispersive model with respect to how the upscaling is performed and concerning the accuracy with respect to ϵ. In the hyperbolic model, only lowest order terms have been kept, resulting in the diffusion and second order effects to disappear. A similar procedure has been made for the simple upscaled model, but where diffusion terms have been kept. The simple upscaled

model represents the typical modeling choice for geothermal applications, while the hyperbolic model results from a straightforward homogenization with a large Péclet number.

All three models are implemented fully coupled using forward Euler in time and finite differences in space, using $\Delta x = 1/128$ for the spatial discretization and $\Delta t = 10^{-4}$ for the time steps. The second energy equation in the dispersive model, (61), is for stability reasons discretized using backward Euler. Spatial derivatives are handled with central differences for second order derivatives, and upstream approximation for first order derivatives. Due to the nonlinearities in the time derivatives and the velocity couplings, the resulting discretized systems are non-linear and Newton's method is applied at each time step to solve the non-linear systems of equations. The initial state is a system in equilibrium where no flow, dissolution or precipitation is occurring. The temperatures are shifted such that they attain values between 0 and 1. With our choice of solubility product, we have

$$T_{fe} = T_{ge} = 1, \quad u_e = 0.5, \quad \bar{q}_e = 0, \quad d_e = 0.25,$$

where the initial pressure is such that no flow is achieved. In the simulations, we consider a case mimicking flow through a pore in a geothermal reservoir where colder fluid is flowing in at $x = 0$, and where the in-situ fluid flows out at $x = 1$. Hence, our boundary conditions are

$$T_{fe} = 0, \quad \partial_x T_{ge} = 0, \quad u_e = 0.5, \quad \bar{q}_e = 1, \quad \partial_x d_e = 0, \text{ at } x = 0,$$

and

$$\partial_x T_{fe} = 0, \quad \partial_x T_{ge} = 0, \quad \partial_x u_e = 0, \quad \partial_x \bar{q}_e = 0, \quad \partial_x d_e = 0, \text{ at } x = 1,$$

and where the boundary conditions for pressure are such that the flow conditions are fulfilled. Simulations with fixed pressure at both ends of the strip were also performed, but the comparisons in the below figures are qualitatively the same. For the simple upscaled and the hyperbolic model, the initial and boundary conditions for T_e correspond to the conditions for T_{fe} given here. Note that the injected ion concentration is the same as the initial one. We use the solubility product for $CaCO_3$ obtained from [26], which shows that $CaCO_3$ is a mineral whose solubility increases with decreasing temperatures. Hence, dissolution is expected as we inject a lower fluid temperature. In all simulations, unless otherwise stated, we have used

$$D = 1, \quad \kappa_f = 1, \quad \kappa_g = 1.2, \quad \varsigma = 1, \quad \rho = 1,$$
$$\rho_0 = 2, \quad \beta_{\rho_f} = 0.01, \quad \beta_\mu = 0.01, \quad k = 1.$$

Figures 2, 3 and 4 show the temperatures and grain widths for the three models with $\epsilon = 0.05$, $\epsilon = 0.01$ and $\epsilon = 0.001$, respectively. All plots are snapshots at $t = 0.7$.

In Figure 2 we see some discrepancy between the models. All models predict dissolution due to the cooling, but there are some difference in the extent of dissolution, which causes differences in the flow conditions, which again affects the heat convection. The simple upscaled model produces quite similar temperatures as the upscaled dispersive model, but differs more in grain width. We separate between fluid and grain temperature in the dispersive model, but even for this large value of ϵ the two temperatures are virtually the same. Decreasing the value of ϵ in Figure 3, we see that the models produce more similar results. This is as expected as both the dispersive model and the simple upscaled behave more like a hyperbolic model for lower values of ϵ. For $\epsilon = 0.01$, the largest difference between the models are found in the temperature profiles. The temperature profile in the hyperbolic model deviates quite a lot from the other two models, indicating the heat conduction still being relevant, despite the model being convection dominated. Applying $\epsilon = 0.001$ shows that the three models produce virtually the same results, as seen in Figure 4. Letting ϵ approach zero in the model equations in the dispersive model and the simple upscaled model, results in the hyperbolic model.

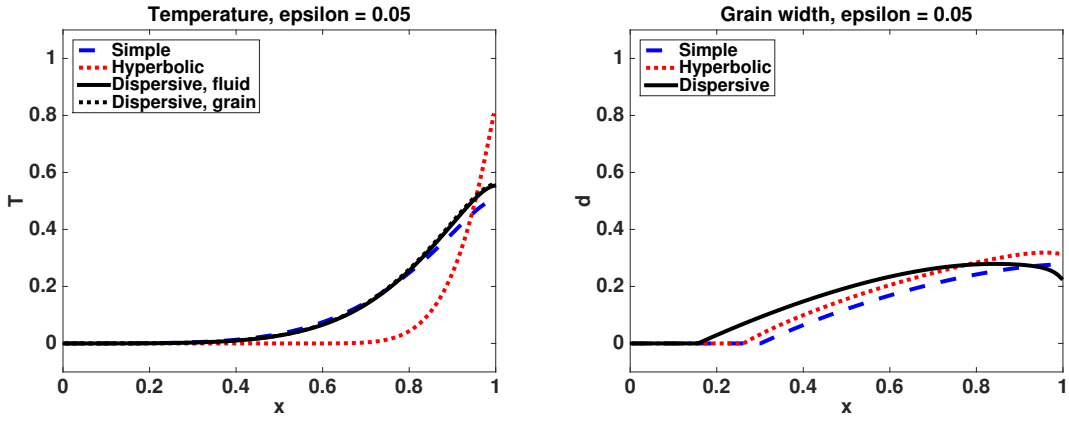

Figure 2: Plots of temperature and grain width, respectively, when $\epsilon = 0.05$. The black solid line refers to the upscaled dispersive model, the dashed blue is the simple upscaled, while the dotted red is the hyperbolic model. The temperature figure also includes a black dotted line, which is the grain temperature in the upscaled dispersive model.

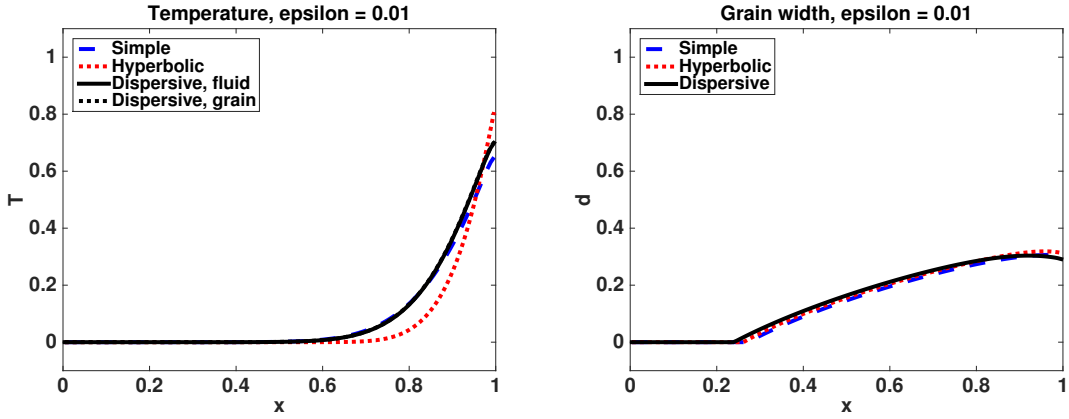

Figure 3: Plots of temperature and grain width, respectively, when $\epsilon = 0.01$. The black solid line refers to the upscaled dispersive model, the dashed blue is the simple upscaled, while the dotted red is the hyperbolic model. The temperature figure also includes a black dotted line, which is the grain temperature in the upscaled dispersive model.

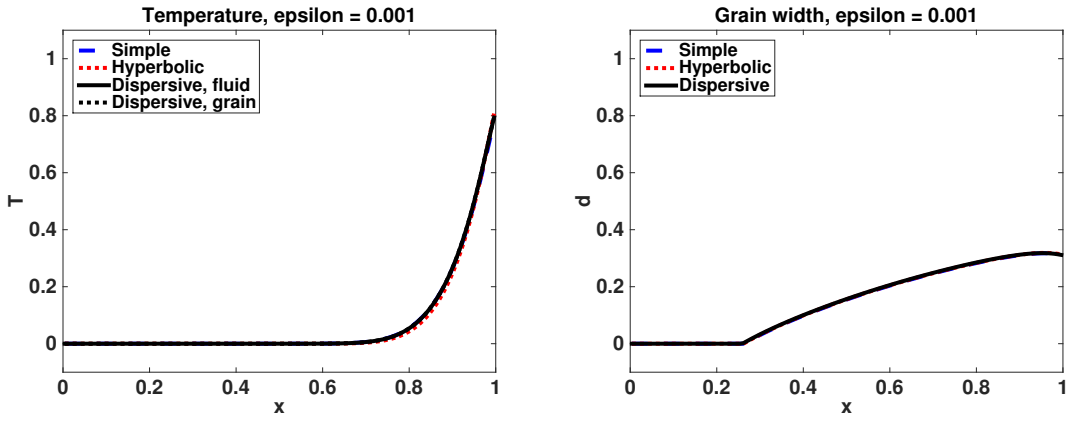

Figure 4: Plots of temperature and grain width, respectively, when $\epsilon = 0.001$. The black solid line refers to the upscaled dispersive model, the dashed blue is the simple upscaled, while the dotted red is the hyperbolic model. The temperature figure also includes a black dotted line, which is the grain temperature in the upscaled dispersive model.

4.2 Fixed geometry vs variable geometry

To investigate the effect of the varying geometry in the upscaling process, we compare the dispersive model (56)-(61) with a model where the changes in geometry due to the chemical reactions are neglected. The dominating convection is included and we keep dispersion terms in the upscaling process. To avoid confusion, we will denote the two models for the fixed geometry model and the variable geometry model in this section. When fixing the geometry the mineral surface concentration v_e is used as a variable instead of the mineral width d_e. The upscaled system of equations consists of five unknowns; u_e, $\bar{q}_e$, v_e, p_e and T_e and five equations to describe them. All equations are defined for $0 \leq x \leq 1$, $t > 0$, and are given by

$$\bar{q}_e = -\frac{1}{12}\frac{\partial_x p_e}{\mu_{fe}}(1 - \epsilon\frac{1}{1260}\frac{\rho_{fe}\beta_\mu}{\kappa_f \mu_{fe}}\partial_x T_e \frac{\partial_x p_e}{\mu_{fe}});$$

$$\partial_t \rho_{fe} + \partial_x(\rho_{fe}\bar{q}_e) = -\epsilon\frac{\beta_{\rho_f}}{\kappa_f}\partial_x\Big(\frac{\bar{q}_e^2}{210}\rho_{fe}\partial_x T_e\Big);$$

$$\begin{aligned}\partial_t v_e &= f_p(T_e, u_e) - f_d(T_e, u_e, v_e)\\ &+ \epsilon\Big((\partial_1 f_p - \partial_1 f_d)\frac{\bar{q}_e}{60\kappa_f}\rho_{fe}\partial_x T_e + \partial_2 f_p(\frac{\bar{q}_e}{60D}(\partial_x u_e - \frac{u_e}{\rho_{fe}}\partial_x\rho_{fe}) - \frac{1}{6D}\partial_t v_e)\Big);\end{aligned}$$

$$\partial_t(u_e + 2v_e) + \partial_x(u_e\bar{q}_e) = \epsilon D\partial_x\Big(\partial_x u_e(1 + \frac{\bar{q}_e^2}{210D^2}) - \frac{\bar{q}_e^2}{210D^2}\frac{u_e}{\rho_{fe}}\partial_x\rho_{fe} - \frac{\bar{q}_e}{30D^2}\partial_t v_e\Big);$$

$$\partial_t(\rho_{fe}T_e) + \partial_x(\rho_{fe}T_e\bar{q}_e) = \epsilon\kappa_f\partial_x\Big(\partial_x T_e(1 + \frac{\bar{q}_e^2}{210\kappa_f^2}(\rho_{fe} - \beta_{\rho_f}T_e)\rho_{fe})\Big),$$

together with (62) for fluid density and viscosity. The derivation of the equations can be found in Appendix A. When the mineral density increases, the changes in the deposited mineral layer will be smaller. To understand when changes in geometry should be accounted for and when they can be neglected, we show the temperature profiles for two choices of ρ in the variable geometry model and fixed geometry model. The boundary and initial conditions for flow, ions and temperature are the same as earlier, where the conditions for fluid temperature is applied for T_e. For initial condition we assume $d_e = 0.25/\rho$ in the variable geometry case and $v_e = 0.25$ in the fixed geometry model, which corresponds to the same amount of minerals in both cases.

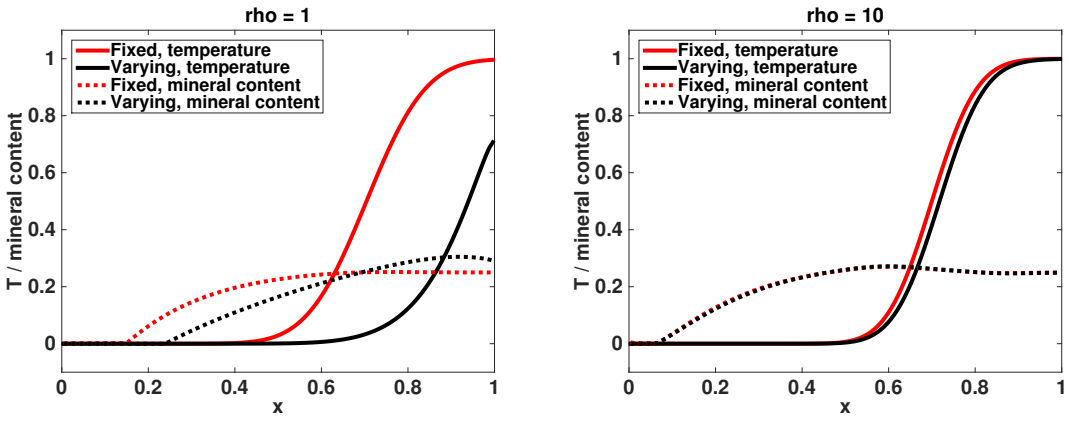

Figure 5: Comparison of the temperature profiles and mineral content for $\rho = 1$ and $\rho = 10$, respectively. The solid lines refer to temperature, where black is for the varying geometry and red for the fixed geometry. The dotted lines refer to the mineral content, where black is for ρd_e for the varying geometry and red is v_e for the fixed geometry.

The boundary conditions for v_e is $\partial_x v_e = 0$ at $x = 0$ and $x = 1$. As earlier, both models are implemented using finite differences with $\Delta x = 1/128$ in space and forward Euler with $\Delta t = 10^{-4}$ in time, and where Newton's method is applied at each time step to solve the resulting nonlinear systems of equations.

Figure 5 compares the temperature profiles and the surface concentration v_e with ρd_e for $\rho = 1$ and $\rho = 10$. There is a large difference in temperature profiles for $\rho = 1$, which is due to the flow velocity through the channel has varied between the models. The different velocity profiles also affect how the minerals dissolve due to different ion transport. For $\rho = 10$, both temperature profile and mineral content are very similar. Hence, when $\rho = 1$, the effect of changing geometry is so large, especially on the temperature profile, that the varying geometry cannot be neglected. Increasing ρ indicates smaller differences between the models.

5 Summary and discussion

Through homogenization, we have derived an upscaled model for reactive flow with heat transfer in a thin strip where convection is dominating, and taken into account changes in aperture caused by the reactions. The effective model includes dispersive terms in both the energy conservation equations and the ion concentration equation, and the model equations include several second order effects arising from the free boundary and the dominating convection. Especially, we find the flow equation to be non-Darcy due to non-isothermal effects arising from the viscosity.

The upscaled model is derived using a simple geometry, but the resulting model provides qualitative information concerning how the various physical processes are coupled under the assumption of varying geometry and large Péclet number. Motivated by the similarities between the upscaled models in [7] and [8], which considers moderate Péclet numbers in a thin strip and in a periodic porous medium, respectively, we expect an extension of the present model to a periodic case to give qualitatively the same couplings of the model as found here. The approach for upscaling a periodic porous medium follows the same ideas as in the thin strip case, although some considerations regarding the geometry are required, especially due to the need of a level set formulation for the free boundary. The present work shows how the various physical processes are coupled and provides information about second order effects due to temperature dependencies, varying geometry and the large Péclet number. This information could be incorporated into a simulator code such as TOUGHREACT [39], which mainly uses simplified expressions for permeability and diffusion although a varying porosity is allowed. TOUGHREACT does not include Taylor

dispersion nor any non-Darcy effects on the fluid flow.

By comparing the upscaled model with two simpler versions; one including simple diffusion and one hyperbolic model, we have investigated numerically the differences between them. For moderately small values of ϵ (that is, around 0.05), the models produce significantly different results, while the differences become smaller when ϵ decreases. For the temperature profile, which is very important in a geothermal setting, we found larger differences between the models. When ϵ decreases, the three models produce very similar results as the model problem is then highly hyperbolic. This investigation shows when and how much the Taylor dispersion influences the outcome of the simulations and gives information about when Taylor dispersion in a convection dominated model should be included and when it can be disregarded.

The upscaled dispersive model is also compared with model equations derived from a fixed geometry pore scale model. By varying the mineral density ρ we investigated the differences between the two models. This comparison shows that for moderate values of the mineral density, the chemical reactions cause changes in the aperture that should not be neglected. Especially for the temperature profile there is a large difference between the models due to the flow velocity through the pore channel not being satisfactory depicted by the fixed geometry model in this case. However, when ρ is large, the changes in aperture become smaller and less important, and the fixed geometry model produces acceptable results.

Acknowledgements

The authors would like to thank K. Kumar for the comments on the numerical results.

F.A. Radu and I.S. Pop would like to acknowledge the support from Statoil through the Akademia agreement.

F.A. Radu would like to acknowledge the support from the Netherlands Organisation for Scientific Research (NWO Visitors Grant 040.11.499) received for the final part of this work.

C. Bringedal and I. Berre would like to acknowledge the support from Research Council of Norway (grant number 228832).

A Upscaled equations for the fixed geometry case

We give a short derivation of the upscaled equations when the width of the strip does not change. The surface concentration v^ϵ is the variable tracking how much mineral is dissolved or precipitated. The fixed 2D domain

$$\Omega^\epsilon = \{(x, y) \in R^2 \mid 0 \leq x \leq 1, -1/2 \leq y \leq 1/2\},$$

with horizontal boundary

$$\Gamma^\epsilon = \{(x, y) \in R^2 \mid 0 \leq x \leq 1, y = \pm 1/2\}$$

is considered. The following non-dimensional system of equations describes the reactive flow and heat transport with dominating convection in the domain:

$$\partial_t u^\epsilon = \nabla \cdot (\epsilon D \nabla u^\epsilon - u^\epsilon \mathbf{q}^\epsilon) \text{ in } \Omega^\epsilon, \tag{73}$$

$$\partial_t \rho_f = -\nabla \cdot (\rho_f \mathbf{q}^\epsilon) \text{ in } \Omega^\epsilon, \tag{74}$$

$$\begin{aligned}\epsilon^2\Big(\partial_t(\rho_f \mathbf{q}^\epsilon) + \nabla \cdot (\rho_f \mathbf{q}^\epsilon \mathbf{q}^\epsilon)\Big) &= -\nabla p^\epsilon \\ &+\epsilon^2\Big(\nabla \cdot \Big(\mu(\nabla \mathbf{q}^\epsilon + (\nabla \mathbf{q}^\epsilon)^T)\Big) - \frac{2}{3}\nabla(\mu \nabla \cdot \mathbf{q}^\epsilon)\Big) \text{ in } \Omega^\epsilon,\end{aligned} \tag{75}$$

$$\partial_t(\rho_f T^\epsilon) = \nabla \cdot (\epsilon \kappa_f \nabla T^\epsilon - \rho_f T^\epsilon \mathbf{q}^\epsilon) \text{ in } \Omega^\epsilon, \tag{76}$$

$$\partial_t v^\epsilon = f_p(T^\epsilon, u^\epsilon) - f_d(T^\epsilon, u^\epsilon, v^\epsilon) \text{ on } \Gamma^\epsilon, \tag{77}$$

$$-\epsilon \mathbf{n}^\epsilon \cdot (D \nabla u^\epsilon) = \partial_t v^\epsilon \text{ on } \Gamma^\epsilon, \tag{78}$$

$$\mathbf{q}^\epsilon = 0 \text{ on } \Gamma^\epsilon, \tag{79}$$

$$-\epsilon \mathbf{n}^\epsilon \cdot (\kappa_f \nabla T^\epsilon) = 0 \text{ on } \Gamma^\epsilon, \tag{80}$$

where the reaction rates are the same as earlier, but using the surface concentration v^ϵ in stead of the grain width d^ϵ to indicate if there are any minerals left in the dissolution rate expression. As earlier, we assume linear dependence between fluid density and viscosity with the fluid temperature. Note that our model does not include an explicit grain part and hence no grain temperature. Alternatively, the presence of a non-reactive solid could have been included by defining a domain with grain temperature. In that case, the boundary conditions stated above would be at the (non-moving) interface between void space and solid, and the last boundary condition would be a heat-flux continuity condition between fluid and grain temperature. The unit normal for the lower part is $\mathbf{n}^\epsilon = -1\mathbf{j}$.

We use the same asymptotic expansions as before, but note that v^ϵ is a function of x and t only as it is only defined on the horizontal boundaries. Inserting the asymptotic expansions into (74) and (79), and collecting the lowest order terms, result, as earlier, in

$$q_0^{(2)} \equiv 0.$$

Integrating (74) over the thin section $Y = \{(x, y) \in R^2 \mid x_1 \le x \le x_1 + \delta x, -1/2 \le y \le 1/2\}$ and performing the same steps as in Section 3.1, result in

$$\partial_t \rho_{fe} + \partial_x(\rho_{fe} \bar{q}_e) = \epsilon \beta_{\rho_f} \partial_x \Big(\int_{-1/2}^{1/2} T_1 q_0^{(1)} dy - \bar{T}_1 \bar{q}_0 \Big). \tag{81}$$

Inserting the asymptotic expansions into (75) and using (79), show as before that p_0 and p_1 are functions of x and t only, and that

$$\partial_x p_0 = \mu_{f0} \partial_y^2 q_0^{(1)} \tag{82}$$

$$\partial_x p_e = \mu_{fe} \partial_y^2 q_e - \epsilon \beta_\mu \partial_y \Big((T_1 - \bar{T}_1) \partial_y q_0^{(1)} \Big) + O(\epsilon^2). \tag{83}$$

Integrating (82) twice and applying the lowest order of (79), show that

$$q_0^{(1)} = -\frac{1}{2} \frac{\partial_x p_0}{\mu_{f0}} (\frac{1}{4} - y^2), \tag{84}$$

$$\bar{q}_0 = -\frac{1}{12} \frac{\partial_x p_0}{\mu_{f0}}. \tag{85}$$

Inserting (84) into (83) and integrating twice yield

$$\frac{1}{2} \partial_x p_e (y^2 - \frac{1}{4}) = \mu_{fe} q_e - \epsilon \beta_\mu \frac{\partial_x p_0}{\mu_{f0}} \int_{-1/2}^{y} \Big(T_1(x, z, t) - \bar{T}_1(x, t) \Big) z dz + O(\epsilon^2). \tag{86}$$

Using the lowest order terms from (73) and (78), we can show that u_0 is a function of x and t only. By integrating (73) over y, interchanging the order of integration and differentiation as before and apply the boundary condition (78), we find that

$$\partial_t(u_e + 2v_e) + \partial_x(u_e\bar{q}_e) = \epsilon D\partial_x^2 u_e - \epsilon\partial_x\Big(\int_{-1/2}^{1/2} u_1 q_0^{(1)} dy - \bar{u}_1\bar{q}_0\Big) + O(\epsilon^2), \tag{87}$$

where $v_e = v_0 + \epsilon v_1$ is the effective surface concentration of the mineral and is by definition a function of x and t only. To proceed, an explicit expression for u_1 is needed. We use similar steps as in Section 3.3: Using the second lowest order terms from (73) and rewriting using (74) yield

$$\partial_t u_0 - \frac{u_0}{\rho_{f0}}\partial_t\rho_{f0} + q_0^{(1)}(\partial_x u_0 - \frac{u_0}{\rho_{f0}}\partial_t\rho_{f0}) = D\partial_y^2 u_1,$$

with boundary conditions

$$D\partial_y u_1 = \partial_t v_0 \text{ at } y = -\frac{1}{2},\ -D\partial_y u_1 = \partial_t v_0 \text{ at } y = \frac{1}{2}$$

coming from (78). We calculate the average over y of the above equation and subtract it, resulting in

$$D\partial_y^2 u_1 = \frac{A}{2}(y^2 - \frac{1}{12}) - 2\partial_t v_0,$$

where $A(x,t) = (\partial_x u_0 - \frac{u_0}{\rho_{f0}}\partial_x\rho_{f0})\frac{\partial_x p_0}{\mu_{f0}}$. Integrating twice with respect to y yields

$$u_1(x,y,t) = u_1|_{y=-1/2} + \frac{1}{24}\frac{A}{D}(y^4 - \frac{1}{2}y^2 + \frac{1}{16}) - \partial_t v_0(y^2 - \frac{1}{4}),$$

which has the average value

$$\bar{u}_1(x,t) = u_1|_{y=-1/2} + \frac{1}{720}\frac{A}{D} + \frac{1}{6}\partial_t v_0.$$

Inserting these two expressions together with (84) and (85) into (87) and evaluating the integral, result in

$$\begin{aligned}\partial_t(u_e + 2v_e) + \partial_x(u_e\bar{q}_e)& \\ = \epsilon D\partial_x\Big(\partial_x u_e(1 + \frac{\bar{q}_e^2}{210D^2}) - \frac{\bar{q}_e^2}{210D^2}\frac{u_e}{\rho_{fe}}\partial_t\rho_{fe} - \frac{\bar{q}_e}{30D^2}\partial_t v_e\Big) + O(\epsilon^2).&\end{aligned}$$

Performing the same steps on (76) and (80), we can show that T_0, and hence ρ_{f0} and μ_{f0}, are independent of y. By integrating (76) over y, interchanging differentiation and integration, applying (80) and inserting expansions, we obtain

$$\begin{aligned}\partial_t(\rho_{fe}T_e) + \partial_x(\rho_{fe}T_e\bar{q}_e) = \epsilon\kappa_f\partial_x^2 T_e& \\ - \epsilon\partial_x\Big((\rho_{f0} - \beta T_{f0})(\int_{-1/2}^{1/2} T_1 q_0^{(1)} dy - \bar{T}_1\bar{q}_0)\Big) + O(\epsilon^2).&\end{aligned} \tag{88}$$

To find an explicit expression for T_1, we use the second lowest order terms from (76), which is rewritten using (74); hence,

$$\rho_{f0}\partial_t T_0 + \rho_{f0}q_0^{(1)}\partial_x T_0 = \kappa_f\partial_x^2 T_1.$$

This equation is manipulated in the same manner as we did with the u_1-equation, resulting in

$$T_1(x,y,t) = T_1|_{y=-1/2} + \frac{1}{24}\frac{C}{\kappa_f}(y^4 - \frac{1}{2}y^2 + \frac{1}{16}) \tag{89}$$

with average

$$\bar{T}_1(x,t) = T_1|_{y=-1/2} + \frac{1}{720}\frac{C}{\kappa_f}, \tag{90}$$

where $C(x,t) = \rho_{f0}\partial_x T_0 \frac{\partial_x p_0}{\mu_{f0}}$. Inserting (89) and (90) together with (84) and (85) into (88) and evaluating the integral, result in

$$\partial_t(\rho_{fe}T_e) + \partial_x(\rho_{fe}T_e\bar{q}_e) = \epsilon\kappa_f\partial_x\Big(\partial_x T_e(1 + \frac{\bar{q}_e^2}{210\kappa_f^2}(\rho_{fe} - \beta_{\rho_f}T_e)\rho_{fe})\Big) + O(\epsilon^2).$$

Inserting (89) and (90) into (81) gives the upscaled mass conservation equation

$$\partial_t\rho_{fe} + \partial_x(\rho_{fe}\bar{q}_e) = -\epsilon\frac{\beta_{\rho_f}}{\kappa_f}\partial_x\Big(\frac{\bar{q}_e^2}{210}\rho_{fe}\partial_x T_e\Big) + O(\epsilon^2),$$

while the momentum equation (86) is

$$\bar{q}_e = -\frac{1}{12}\frac{\partial_x p_e}{\mu_{fe}}(1 - \epsilon\frac{1}{1260}\frac{\rho_{fe}\beta_\mu}{\kappa_f\mu_{fe}}\partial_x T_e\frac{\partial_x p_e}{\mu_{fe}}) + O(\epsilon^2).$$

Finally, we upscale (77) by first regularizing the dissolution rate by defining $f_\delta(T^\epsilon, v^\epsilon) = k_0 e^{-\alpha/T^\epsilon} w_\delta(v^\epsilon)$ where w_δ is defined as in (55) and δ is a small, positive number. We Taylor expand the reaction rates around (T_e, u_e, v_e) and obtain

$$\begin{aligned}\partial_t v_e =& f_p(T_e,u_e) - f_d(T_e,u_e,v_e) + \epsilon\Big((\partial_1 f_p - \partial_1 f_d)\frac{\bar{q}_e}{60\kappa_f}\rho_{fe}\partial_x T_e \\ &+ \partial_2 f_p(\frac{\bar{q}_e}{60D}(\partial_x u_e - \frac{u_e}{\rho_{fe}}\partial_x\rho_{fe}) - \frac{1}{6D}\partial_t v_e)\Big) + O(\epsilon^2)\end{aligned}$$

after letting δ approach zero.

References

[1] G. Allaire. Homogenization of the unsteady Stokes equations in porous media. In *Progress in partial differential equations: calculus of variations, applications (Pont-à-Mousson, 1991)*, volume 267 of *Pitman Res. Notes Math. Ser.*, pages 109–123. Longman Sci. Tech., Harlow, 1992.

[2] G. Allaire. One-phase Newtonian flow. In *Homogenization and porous media*, pages 45–76. Springer, 1997.

[3] G. Allaire, R. Brizzi, A. Mikelić, and A. Piatnitski. Two-scale expansion with drift approach to the taylor dispersion for reactive transport through porous media. *Chemical Engineering Science*, 65(7):2292–2300, 2010.

[4] G. Allaire and H. Hutridurga. Homogenization of reactive flows in porous media and competition between bulk and surface diffusion. *IMA J. Appl. Math.*, 77(6):788–815, 2012.

[5] G. Allaire, A. Mikelić, and A. Piatnitski. Homogenization approach to the dispersion theory for reactive transport through porous media. *SIAM J. Math. Anal.*, 42(1):125–144, 2010.

[6] J.-L. Auriault and P. M. Adler. Taylor dispersion in porous media: analysis by multiple scale expansions. *Advances in Water Resources*, 18(4):217–226, 1995.

[7] C. Bringedal, I. Berre, I. S. Pop, and F. A. Radu. A model for non-isothermal flow and mineral precipitation and dissolution in a thin strip. *Journal of Computational and Applied Mathematics*, 2014. http://dx.doi.org/10.1016/j.cam.2014.12.009.

[8] C. Bringedal, I. Berre, I. S. Pop, and F. A. Radu. Upscaling of non-isothermal reactive porous media flow with changing porosity. *Transport in Porous Media*, 2015. http://dx.doi.org/10.1007/s11242-015-0530-9.

[9] C. Bringedal, I. Berre, and F. A. Radu. An approach for investigation of geochemical rock-fluid interactions. In *Proceedings, Thirty-Ninth Workshop on Geothermal Reservoir Engineering, Stanford University*, 2014.

[10] H. Bruining, M. Darwish, and A. Rijnks. Computation of the longitudinal and transverse dispersion coefficient in an adsorbing porous medium using homogenization. *Transp. Porous Media*, 91(3):833–859, 2012.

[11] R. Chang and K. A. Goldsby. *General Chemistry, The Essential Concepts*. McGraw-Hill, 2014.

[12] Z. Chen, S. L. Lyons, and G. Qin. Derivation of the forchheimer law via homogenization. *Transport in porous media*, 44(2):325–335, 2001.

[13] A. Fasano. *Mathematical models of some diffusive processes with free boundaries*. Universidad Austral. Departamento de Matemática, 2005.

[14] P. Knabner, C. J. van Duijn, and S. Hengst. An analysis of crystal dissolution fronts in flows through porous media. part 1: Compatible boundary conditions. *Advances in water resources*, 18(3):171–185, 1995.

[15] K. Kumar, T. L. Van Noorden, and I. S. Pop. Effective dispersion equations for reactive flows involving free boundaries at the microscale. *Multiscale Modeling & Simulation*, 9(1):29–58, 2011.

[16] K. S. McLin, K. M. Kovac, J. N. Moore, M. C. Adams, and T. Xu. Modeling the geochemical effects of injection at coso geothermal field, ca; comparison with field observations. In *Proceedings, Thirty-first Workshop on Geothermal Reservoir Engineering, Stanford University*, 2006.

[17] C. C. Mei and J.-L. Auriault. The effect of weak inertia on flow through a porous medium. *J. Fluid Mech.*, 222:647–663, 1991.

[18] A. Mikelić. Homogenization of nonstationary navier-stokes equations in a domain with a grained boundary. *Annali di Matematica pura ed applicata*, 158(1):167–179, 1991.

[19] A. Mikelić, V. Devigne, and C. J. van Duijn. Rigorous upscaling of the reactive flow through a pore, under dominant Peclet and Damkohler numbers. *SIAM J. Math. Anal.*, 38(4):1262–1287, 2006.

[20] A. Mikelić and C. Rosier. Rigorous upscaling of the infinite adsorption rate reactive flow under dominant Péclet number through a pore. *Annali Dell'Universita'Di Ferrara*, 53(2):333–359, 2007.

[21] A. Mikelić and C. J. van Duijn. Rigorous derivation of a hyperbolic model for Taylor dispersion. *Math. Models Methods Appl. Sci.*, 21(5):1095–1120, 2011.

[22] E. K. Mroczek, S. P. White, and D. J. Graham. Deposition of amorphous silica in porous packed beds $\tilde{\text{N}}$ predicting the lifetime of reinjection aquifers. *Geothermics*, 29(6):737–757, 2000.

[23] H. Pape, C. Clauser, J. Iffland, R. Krug, and R. Wagner. Anhydrite cementation and compaction in geothermal reservoirs: Interaction of pore-space structure with flow, transport, p-t conditions, and chemical reactions. *International Journal of Rock Mechanics and Mining Sciences*, 42(7):1056–1069, 2005.

[24] S. Patankar. *Numerical heat transfer and fluid flow.* McGraw-Hill, 1980.

[25] M. A. Peter. Coupled reaction–diffusion processes inducing an evolution of the microstructure: Analysis and homogenization. *Nonlinear Analysis: Theory, Methods & Applications*, 70(2):806–821, 2009.

[26] L. N. Plummer, D. L. Parkhurst, G. W. Flemming, and S. A. Dunkle. A computer program incorporating pitzer's equations for calculation of geochemical reactions in brines, 1988.

[27] N. Ray, T. van Noorden, F. A. Radu, W. Friess, and P. Knabner. Drug release from collagen matrices including an evolving microstructure. *ZAMM-Journal of Applied Mathematics and Mechanics*, 93(10-11):811–822, 2013.

[28] E. Sonnenthal, A. Ito, N. Spycher, M. Yui, J. Apps, Y. Sugita, M. Conrad, and S. Kawakami. Approaches to modeling coupled thermal, hydrological, and chemical processes in the drift scale heater test at yucca mountain. *International Journal of Rock Mechanics and Mining Sciences*, 42(5):698–719, 2005.

[29] L. Tartar. Incompressible fluid flow in a porous medium - convergence of a homogenization process. In E. Sanchez-Palencia, editor, *Non-Homogeneous Media and Vibration Theory*, volume 129, pages 368–377. Springer, 1980.

[30] G. Taylor. Dispersion of soluble matter in solvent flowing slowly through a tube. In *Proceedings of the Royal Society of London A: Mathematical, Physical and Engineering Sciences*, volume 219, pages 186–203. The Royal Society, 1953.

[31] C. J. van Duijn and P. Knabner. Travelling wave behavior of crystal dissolution in porous media flow. *European Journal of Applied Mathematics*, 8:49–72, 1997.

[32] C. J. van Duijn and I. S. Pop. Crystal dissolution and precipitation in porous media: pore scale analysis. *Journal f§r die reine und angewandte Matematik*, 577:171–211, 2004.

[33] T. L. van Noorden. Crystal precipitation and dissolution in a porous medium: effective equations and numerical experiments. *Multiscale Modeling & Simulation*, 7(3):1220–1236, 2009.

[34] T. L. van Noorden. Crystal precipitation and dissolution in a thin strip. *European Journal of Applied Mathematics*, 20:69–91, 2009.

[35] T. L. van Noorden, I. S. Pop, A. Ebigbo, and R. Helmig. An upscaled model for biofilm growth in a thin strip. *Water Resources Research*, 46(6), 2010.

[36] T. L. van Noorden, I. S. Pop, and M. Röger. Crystal dissolution and precipitation in porous media: L1-contraction and uniqueness. In *Discrete Contin. Dyn. Syst.,(Dynamical Systems and Differential Equations. Proceedings of the 6th AIMS International Conference, suppl.)*, pages 1013–1020, 2007.

[37] R. Wagner, M. Kühn, V. Meyn, H. Pape, U. Vath, and C. Clauser. Numerical simulation of pore space clogging in geothermal reservoirs by precipitation of anhydrite. *International Journal of Rock Mechanics and Mining Sciences*, 42(7):1070–1081, 2005.

[38] S. P. White and E. K. Mroczek. Permeability changes during the evolution of a geothermal field due to the dissolution and precipitation of quartz. *Transport in porous media*, 33(1-2):81–101, 1998.

[39] T. Xu, N. Spycher, E. Sonnenthal, L. Zheng, and K. Pruess. TOUGHREACT user's guide: A simulation program for non-isothermal multiphase reactive transport in variably saturated geologic media, version 2.0. *Earth Sciences Division, Lawrence Berkeley National Laboratory, Berkeley, USA*, 2012.

PREVIOUS PUBLICATIONS IN THIS SERIES:

Number	Author(s)	Title	Month
15-28	J.H.M. Evers S.C. Hille A. Muntean	Measure-valued mass evolution problems with flux boundary conditions and solution-dependent velocities	July '15
15-29	B.S. van Lith J.H.M. ten Thije Boonkkamp W.L. IJzerman	Embedded WENO: a design method to improve existing WENO schemes	July '15
15-30	S.W. Gaaf M.E. Hochstenbach	Probabilistic bounds for the matrix condition number with extended Lanczos bidiagonalization	Sept. '15
15-31	G.A. Bonaschi P.J.P. van Meurs M. Morandotti	Dynamics of screw dislocations: A generalised minimising-movements scheme approach	Sept. '15
15-32	C. Bringedal I. Berre I.S. Pop F.A. Radu	Upscaling of non-isothermal reactive porous media flow under dominant Péclet number: the effect of changing porosity	Oct. '15

Ontwerp: de Tantes,
Tobias Baanders, CWI